UNIVERSITY OF CALIFORNIA
RIVERSIDE

Deep Sea Sediment Alteration Across the Paleocene-Eocene Thermal Maximum

A Dissertation submitted in partial satisfaction
of the requirements for the degree of

Doctor of Philosophy

in

Earth and Planetary Sciences

by

Michelle Zill

June 2022

Dissertation Committee:
Dr. Sandra Kirtland Turner, Chairperson
Dr. Mary L. Droser
Dr. Andy Ridgwell

The Dissertation of Michelle Zill is approved:

_____

_____

_____

Committee Chairperson

University of California, Riverside

AKNOWLEDGMENTS

The competition of this project would not have been possible without the assistance and direction of my two co-advisors Dr. Sandra Kirtland Turner and Dr. Mary Droser. In my time at UCR, I have grown significantly as a scientist and as a person, due to the support from both of you. I would like to thank Dr. Andy Ridgwell for serving on my committee and providing thoughtful comments throughout my time at UCR. I would like to thank Dr. Peter Sadler for his helpful discussion when formulating my projects and leading my qualification committee.

Being part of two labs throughout my graduate career, I must also thank a long list of people from the Droser and Kirtlander Turner/Ridgwell lab groups for their assistance throughout my time at UCR including Chrissy Hall, Aaron Martinez, Scott Evans, Bridget Kelly, Rachel Surprenant, Pam Vervoot, Dominik Huelse, Yoshiki Kanzaki, and Allison Keller. I would like to thank my family for providing endless support and encouragement, especially throughout the challenges of the pandemic.

This research was supported by an award from the Heising-Simons Foundation to Sandra Kirtland Turner, Andy Ridgwell, and Lee Kump as well as through grants from the Geological Society of America, University of California, Riverside Gradate Division, and University of California, Riverside Environmental Dynamics and GeoEcology (EDGE) Institute.

ABSTRACT OF THE DISSERTATION

Deep Sea Sediment Alteration Across the Paleocene-Eocene Thermal Maximum

by

Michelle Zill

Doctor of Philosophy, Graduate Program in Earth and Planetary Sciences
University of California, Riverside, June 2022
Dr. Sandra Kirtland Turner, Chairperson

Traces of past oceanic and environmental conditions are stored in deep sea sediments as 'proxy records'. When these 'proxy records' are deciphered, they can contain valuable information that can be used to reconstruct past chemical and physical conditions of the ocean throughout time. Though, these records can be distorted by a variety of chemical, physical, and biological processes including bioturbation, dissolution, and variations in sedimentation rate, complicating the relationship between stratigraphic depth and age of a geochemical proxy, and making it more difficult to translate past climates and environments. As CO_2 levels continue to rise in our atmosphere, an understanding of how past extreme warming events, such as the Paleocene-Eocene Thermal Maximum (PETM, ~55.9 Ma), impacted environmental conditions and ecosystem dynamics can better inform how our modern ocean ecosystems will react to anthropogenic warming.

During the PETM, a rapid injection of isotopically light carbon into the ocean and/or atmosphere, indicated by a negative carbon isotope excursion (CIE), resulted in global warming, changes in ocean ecosystem dynamics including a severe benthic

foraminifera extinction, and global dissolution of deep-sea carbonates due to shoaling of the calcite compensation depth (CCD). This subsequent dissolution erased the onset of the PETM CIE at many deep sea locations, while the impact on the deep sea macrobenthic community remains unexplored.

In this dissertation I investigate the response of the deep sea benthic and infaunal macrofauna response to the PETM by quantifying bioturbation intensity utilizing the ichnofabric index (ii) by identifying and measuring trace fossil community change in 46 deep sea sediment cores. I find global decreases in trace fossil community size, with over half of the locations ceasing bioturbation following the onset of the PETM. I utilize a novel burrow-specific sampling technique to investigate the movement of bulk sediment within discrete trace fossils. I find the most significant impact on the geochemical record occurs in concurrence with the CIE. I utilize neodymium isotopes in the North Atlantic at IODP site U1403 to investigate circulation patterns and find no change from Southern dominated deep water formation throughout the PETM.

Table of Contents

List of Figures

Chapter 1

Chapter 2

Chapter 3

List of Tables

Chapter 1

INTRODUCTION

As CO_2 levels continue to rise in our atmosphere, a better understanding of the thresholds controlling the climate system are needed to understand how our icehouse ocean ecosystems will transition into an anthropogenically forced greenhouse world. Some consequences of our rapidly changing climate remain difficult to precisely predict, presenting challenges in preparing for an uncertain future. Studying past intervals during which Earth warmed rapidly in response to a large input of carbon to the atmosphere and ocean systems is one of the best approaches we have for understanding the possible effects of modern climate change (Norris et al. 2013), which can help us prepare for our own uncertain future.

One of the best analogues for anthropogenic climate change is the Paleocene-Eocene Thermal Maximum (PETM), during which a large amount of isotopically light carbon was rapidly injected into the ocean and/or atmosphere. This release of carbon resulted in rapid rise in global temperatures, widespread dissolution in the deep sea, and extinction for many benthic foraminifera (Dunkley Jones et al., 2013; Greene et al., 2019; Kirtland Turner, 2018; McInerney and Wing, 2011).

In the deep sea where sediment deposition is relatively consistent, we find some of the most pristine geological records of our past, in which we find illuminating records of Earth's history in fossil and geochemical records. With slow but steady accumulation rates (~1cm/kyr) and low erosion rates (Sadler 1981), the deep sea preserves exceptional records for high-resolution climate studies. The composition of deep sea sediments are comprised of carbonate ooze, silica ooze, and clay. The proportion of sediment preserved

that is biological in origin is dependent upon local productivity and ocean chemistry. With oozes comprising of at least 30% of biological tests (i.e. coccolithophores, foraminifera tests for carbonate oozes, and radiolarian and diatom tests for silicious oozes), requiring significant local productivity, as only about 1% of the tests of these organism will survive into the sediment record (Cronin 2009). The carbonate chemistry of the ocean also influences the preservation of carbonate tests. The ocean, at a certain depth (~4,500 m in the modern ocean) is undersaturated in carbonate. In undersaturated waters, the tests dissolve, leaving sediments comprised mostly of terrigenous clay.

Two major sources of possible distortion in the sediment record are overturning ocean circulation leading to dissolution, and changes in bioturbation and animal activity within the sediment after deposition. Constraining these variables is vital to understanding past environmental response to extreme warming, and this being able to better predict Earth's future.

Benthic mixing in the deep sea can distort geochemical proxy signals of short-term environmental change. We have a direct record of these activities preserved as ichnofabric- the sediment fabric resulting from all aspects of biological modification of the sediments (Droser and Bottjer 1987). In the deep sea (>1000 mbsf), in the absence of environmental inhibitors, bioturbating organisms effectively "keep up" with slow sediment accumulation (Ekdale et al. 1984), resulting in thoroughly mixed sediments. This has two significant potential implications; first, that bioturbation while leaving a physical record, is also "mixing" the geochemical signal; and second, that the absence of completely bioturbated sediment is indicative of an environmental perturbation causing

the absence or decrease in burrowers. Understanding these implications has critical significance for accurate interpretation of deep sea sediment environments and ocean chemistry.

Scope of Work

In this dissertation I have focused on deep sea sediment alteration through bioturbation and overturning ocean circulation across the PETM. Chapter 1 utilizes trace fossils in deep sea sediments to examine the benthic and infaunal macrofauna to determine occurrence, ecology, and environmental conditions across the global. Chapter 2 tests a novel discrete burrow-specific sampling technique to determine the impact of bioturbating organisms in bulk geochemical records. Chapter 3 addresses post-depositional changes in sedimentary records by investigating changes in ocean circulation utilizing neodymium isotopes to produce a new record from the North Atlantic record, further informing our understanding of deep water sources. By minimizing uncertainty when reconstructing paleoenvironments and paleoclimates, lessons from the past become clearer, better informing our decisions for our future and the coming consequences for warming our planet.

References

Bromley, R. G. (2012). *Trace fossils: biology, taxonomy and applications*. Routledge.

Bruland, K. W. (1983). Trace elements in seawater.

Cronin, T. M. (2009). *Paleoclimates: understanding climate change past and present*. Columbia University Press.

Droser, M. L., & Bottjer, D. J. (1987). Development of ichnofabric indices for strata deposited in high-energy nearshore terrigenous clastic environments.

Droser, M. L., & Bottjer, D. J. 33. TRACE FOSSILS AND ICHNOFABRIC IN LEG 119 CORES1.

Ekdale, A. A., & Bromley, R. G. (1984). Comparative ichnology of shelf-sea and deep-sea chalk. *Journal of Paleontology*, 322-332.

Greene, S. E., Ridgwell, A., Kirtland Turner, S., Schmidt, D. N., Pälike, H., Thomas, E., ... & Hoogakker, B. A. A. (2019). Early Cenozoic decoupling of climate and carbonate compensation depth trends. *Paleoceanography and paleoclimatology*, *34*(6), 930-945.

Jones, T. D., Lunt, D. J., Schmidt, D. N., Ridgwell, A., Sluijs, A., Valdes, P. J., & Maslin, M. (2013). Climate model and proxy data constraints on ocean warming across the Paleocene–Eocene Thermal Maximum. *Earth-Science Reviews*, *125*, 123-145.

McInerney, F. A., & Wing, S. L. (2011). The Paleocene-Eocene Thermal Maximum: A perturbation of carbon cycle, climate, and biosphere with implications for the future. *Annual Review of Earth and Planetary Sciences*, *39*, 489-516.

Norris, R. D., Turner, S. K., Hull, P. M., & Ridgwell, A. (2013). Marine ecosystem responses to Cenozoic global change. *Science*, *341*(6145), 492-498.

Sadler, P. M. (1981). Sediment accumulation rates and the completeness of stratigraphic sections. *The Journal of Geology*, *89*(5), 569-584.

Turner, S. K. (2018). Constraints on the onset duration of the Paleocene–Eocene thermal maximum. *Philosophical Transactions of the Royal Society A: Mathematical, Physical and Engineering Sciences*, *376*(2130), 20170082.

Westerhold, T., Röhl, U., Donner, B., McCarren, H. K., & Zachos, J. C. (2011). A complete high-resolution Paleocene benthic stable isotope record for the central Pacific (ODP Site 1209). *Paleoceanography*, *26*(2).

Zachos, J. C., Röhl, U., Schellenberg, S. A., Sluijs, A., Hodell, D. A., Kelly, D. C., ... & Kroon, D. (2005). Rapid acidification of the ocean during the Paleocene-Eocene thermal maximum. *Science*, *308*(5728), 1611-1615.

Chapter 1: IMPACT OF REDUCED BIOTURBATION ACROSS THE PALEOCENE-EOCENE THERMAL MAXIMUM

Abstract

The Paleocene Eocene Thermal Maximum (PETM, 55.93 Ma) was an abrupt period of greenhouse warming, during which thousands of gigatons of isotopically depleted carbon were added to the atmosphere over the span of a few thousand years, leading to a global negative carbon isotope excursion (CIE) and carbonate dissolution. Differences in bioturbation intensity and trace fossil diversity across the PETM between ocean sites can provide unique insight into the reaction and recovery of the macrofaunal benthic ecosystem across the PETM and may contribute to basin-specific patterns of various geochemical indicators, including carbonate dissolution, changes in ocean oxygenation, and CIE magnitude. Here we investigate the ichnofabric index and ichnology from 46 cores from the International Ocean Discovery Program (IODP) and its predecessors to construct a global picture of deep-sea benthic macrofauna and paleoenvironment across the PETM. We find cessations of bioturbation in over half of the cores investigated, and a global decrease in maximum and average burrow diameter following the PETM onset, indicating a global benthic macrofauna community change and extirpation at many sites. Since we find no global correlations between these changes in burrow sizes and lithological, environmental, paleodepth, or location, we suggest local differences impacted the benthic environment.

Introduction

The Paleocene Eocene Thermal Maximum (PETM, 55.93–55.71 Ma; Westerhold et al., 2017) was a rapid hyperthermal event, characterized by a > 2‰ negative carbon isotope excursion in marine and terrestrial records (Kennett and Stott, 1991; Koch et al., 1992; Dickens et al., 1995; Zachos et al., 2005; Dickens, 2011). Though the mechanism of release and source of carbon is still debated, during the PETM thousands of petagrams of isotopically depleted carbon were released to the ocean/atmosphere system (Zeebe et al., 2009; Meissener et al., 2014; Bowen et al., 2015; Frieling et al., 2016). This release had an extreme effect on the geochemical, biotic, and physical processes, with average sea surface temperatures increasing by ~4°C (Dunkley Jones et al., 2013; Frieling et al., 2017) and deep ocean temperatures increasing by ~6°C (Kennett and Stott, 1991), and widespread ocean acidification, with the lysocline and CCD shoaling by > 2 km (Zachos et al., 2005; Penman et al., 2014; Bralower et al., 2018). All known PETM carbonate sites experienced some dissolution (Wade et al., 2020), with most global sediments shifting from biogenic carbonate-dominated sediments to clay-dominated sediments, but the extent of dissolution was not globally uniform (Penman et al., 2014; Zachos et al., 2005, Wade et al 2020). With increased atmospheric warming due to the high concentration CO_2 in the atmosphere, trade winds weakened, the latitudinal temperature gradient decreased, and ocean ventilation decreased (Winguth et al., 2012; Pälike et al., 2014; Heinze and Ilyina, 2015).

During the PETM, there were major changes in the shallow and deep sea communities, including migrations to higher latitudes, evolutionary radiations, and

extinctions. In the surface ocean, the distribution of planktic foraminifera, dinoflagellates, and radiolarians shifted poleward (Kelly et al., 1996; Thomas and Shackleton, 1996; Crouch et al., 2001; Bralower, 2002; Hollis, 2006; Sluijs et al., 2006; Speijer et al. 2012; Schneider et al., 2013). In the deep sea, the PETM caused a large extinction event of deep-sea benthic foraminifera, impacting 29% of species in the Southern Ocean (Hayek et al. 2019) and 54% of the species in the Northeast Atlantic Ocean (Alegret et al. 2018) within the first 10 kyr of the Eocene (Thomas, 1998; Thomas 2007; Alegret et al., 2010), likely in response to changes temperature, pH, and/or dissolved oxygen (Thomas, 2003; Alegret et al., 2021). Benthic ostracodes dwarfed in carapace size, and changed in assemblage (Sluijs et al., 2007; Webb et al., 2009; Yamaguchi et al. 2012).

Bioturbation, or infaunal activity within the sediments disrupts and can alter the original physical sedimentary record. The intensity and diversity of bioturbation reflects local ecological conditions and can be preserved in the ichnological record as both discrete trace fossils and ichnofabrics. In the deep sea, sedimentation rates can range from 0.01cm/kyr to 3cm/kyr (Lyle, 2016) while sediment homogenization extends up to ~10cm below the water-sediment interface (Bard, 1994; Boudreau 1994; Teal et al., 2008, 2010). Bioturbation in these conditions rework original primary physical sedimentary structures such as laminations as well as erase shallow discrete burrows, unless there are changes in environmental factors such as anoxia, salinity, turbulence, sedimentation rate, sediment composition, or lack of abundance of organic matter (Ekdale et al., 1984, Tarhan 2018).

However, even in completely bioturbated deep-sea sediments, biogenic structures produced by deeper-burrowing infauna and are commonly preserved in the "transition layer" which can extend from 10cm-2m below the sediment-water interface, where sediment mixing shifts from complete homogenization to heterogeneous structure-building by deeper-burrowing organisms (Pemberton et al., 1976, Ekdale et al., 1984; Bromley, 1996, Lobza and Schieber, 1999; Schieber, 2003; Tarhan 2018).

Chondrites, Planolites, Paleophycus, Zoophycos, and *Thalassinoides* are typically preserved trace fossils (Ekdale 1977; Ekdale 1980; Bromely 1990; Droser and Bottjer 1991; Bromely 1996). When used in conjunction with physical sedimentology, ichnological patterns can be helpful in characterizing past environmental and depositional changes that can affect the benthic and infaunal environment (i.e., oxygenation, available nutrients, rate of sedimentation, winnowing etc.) (Wetzel, 1983; Savrda and Bottjer, 1986, 1987, 1989, 1991; Droser and Bottjer, 1991; Savrda, 2007; Rodríguez-Tovar and Uchman, 2010; Wetzel, 2010; Buatois and Mángano, 2011; Uchman and Wetzel, 2011; MacEachern et al. 2012; Wetzel and Uchman, 2012). By examining ichnological features such as bioturbation intensity (through the ichnofabric index), discrete burrow size, and penetration depth, one can assess environmental parameters including oxygenation and benthic nutrient availability (Ekdale and Bromley, 1983, 1991; Bromley and Ekdale, 1986; Taylor and Goldring, 1993; Ekdale et al., 2012; Savrda, 2016). For example, when investigating changes in trace fossils in response to decreasing levels of benthic oxygenation, they find progressively lower trace-fossil diversities, generally associated with decreases in burrow diameters and bioturbation depths (Savrda, 2012).

The majority of deep-sea benthic ecosystem analysis has been mainly focused on microfossil data (benthic foraminifera and ostracode assemblages), while the effects of the PETM on deep-sea macrobenthic communities remain poorly understood. As fossilized deep-sea benthic and infaunal organisms are extremely rare in deep-sea deposits, their communities' dynamics in response to extreme environmental change throughout the PETM remain poorly understood (Speijer et al 2012). Previous investigations into ichnological assemblages and trace fossil abundances of two bathyal sequences show cessations of bioturbation coincident with the onset of the PETM, with delayed recovery of trace fossil diversity and abundance, indicating that these sea-floor communities were exposed to stressed conditions (Nicolo et al., 2010; Rodriguez-Tovar et al., 2011, Speijer et al 2012).

We expand upon these analyses by conducting detailed ichnological analysis on 46 deep-sea sediment cores from all ocean basins to evaluate the impact of the PETM evidenced by lithological and environmental variations on the benthic and infaunal ecosystem dynamics over the PETM. In addition to determining trace fossil abundances and diversity, we determined bioturbation intensity and comprehensive burrow size measurements. These detailed ichnological data in the form of the quantitative bioturbation intensity and trace fossil diversity, can be correlated with paleoclimate and palaeoceanographic proxy records to better understand global deep-sea patterns during the PETM.

Materials

To analyze the impact of bioturbation throughout the PETM, 46 sediment cores spanning the Late Paleocene to the PETM onset with paleodepths ≥1,000 m were selected for this study from the archives of the International Ocean Discovery Program (IODP) and its predecessors (Deep Sea Drilling Project, DSDP; Ocean Drilling Program, ODP; and Integrated Ocean Discovery Program, also IODP). The PETM was identified at each site by the Shipboard Scientific Party or by referral to post-cruise literature (Kelly et al., 2012; Hollis et al., 2015; Frieling et al., 2019; Penman et al., 2019; Shaw et al, 2020; Witkowski et al., 2020). When isotopic records were not available, the Paleocene/Eocene boundary was identified through the benthic foraminiferal extinction which was correlated with the onset of the PETM (Supplemental Table 1.1; Alegret et al. 2009).

Methods

We analyzed 14 cores in-person, and the remaining 32 cores were analyzed utilizing high-resolution images from the IODP image library. Images were adjusted (levels, brightness and vibrance) to best enhance the visibility of burrows and primary sedimentary structures (Rodríguez-Tovar et al., 2015). Bioturbation intensity generally varies widely across temporal and spatial scales due to its sensitivity to environmental factors (McIlroy, 2007). For this reason, bioturbation was assessed in a highly resolved stratigraphic context across each of the PETM sections. The sedimentology, ichnofabric index (ii), and ichnology with depth were logged on all cores in a cm-by-cm grid scale and mm-scale when necessary (Table 1.1).

Table 1.1 Summary of ichnological data and measurements from study.

Program	Leg	Site	Boundary Type	Ichnology Assemblage	Max Difference Pre and PETM	Average Difference Pre and PETM	Boundary Crossing Burrow diameter	Boundary Crossing Burrow Type
DSDP	22	213	1	*Pl*	0.164	0.153		
DSDP	27	259	1	*Pl*	0.196	0.208		
DSDP	29	277	1	*Pl*	0.166	0.174		
DSDP	32	305	1	*Pl*	0.04	0.067		
DSDP	48	401	1	*Pl, Pa*	0.142	0.151		
DSDP	74	525	3	*Pl, Pa*	0.329	0.341		
DSDP	74	527	2	*Pl, Pa*	0.208	0.229	0.18	*Pl*
DSDP	80	549	1	*Pl, Pa*	0.131	0.156		
DSDP	86	577	1	*Pl*	0.32	0.154		
ODP	113	689	1	*Pl, Pa*	N/A	N/A		
ODP	113	690B	1	*Pl, Pa*	0.123	0.13		
ODP	119	738	3	*Pl, Pa*	0.298	0.315		
ODP	143	865	1	*Pl*	0.144	0.151		
ODP	159	959	1	*Pl, Pa*	0.16	0.156		
ODP	165	999	4	*Pl, Ch*	0.356	0.343		
ODP	165	1001A	3	*Pl, Pa, Ch, Zo*	0.242	0.256		
ODP	165	1001B	3	*Pl, Pa, Ch, Zo*	0.235	0.246		
ODP	171 B	1051B	1	*Pl*	0.239	0.207		
ODP	183	1135	1	*Pl, Pa*	0.174	0.161		
ODP	189	1172	1	*Pl, Pa*	0.161	0.161		
ODP	198	1209B	2	*Pl*	0.2143	0.2193	0.296	*Pl*
ODP	198	1210	2	*Pl, Th*	0.2565	0.2575	0.307	*Th*
ODP	198	1211	1	*Pl*	0.216	0.221		
ODP	198	1212	2	*Pl*	0.2525	0.2475	0.329	*Pl*
ODP	199	1215	1	*Pl*	0.2375	0.2195		
ODP	199	1220B	3	*Pl*	0.2148	0.3078		
ODP	199	1221C	1	*Pl, Pa*	0.162	0.144		
ODP	199	1221D	1	*Pl, Pa*	0.14	0.143		
ODP	207	1258A	3	*Pl,Ch*	0.218	0.307		
ODP	207	1258C	3	*Pl, Ch*	0.285	0.296		

ODP	207	1259A	2	*Pl, Ch*	0.177	0.172	0.229	*Pl*
ODP	207	1259B	2	*Pl, Ch*	0.187	0.175	0.173	*Pl*
ODP	207	1259C	2	*Pl, Ch*	0.186	0.207	0.182	*Pl*
ODP	207	1260A	4	*Pl, Ch*	0.3905	0.3725		
ODP	207	1260B	4	*Pl, Ch*	0.341	0.329		
ODP	208	1262A	2	*Pl, Pa, Ch*	0.23	0.23	0.216	*Pl*
ODP	208	1262B	2	*Pl, Pa, Ch*	0.233	0.232	0.267	*Pl*
ODP	208	1263A	3	*Pl, Ch*	0.265	0.263		
ODP	208	1263C	3	*Pl, Ch*	0.321	0.326		
ODP	208	1263D	3	*Pl, Ch*	0.311	0.323		
ODP	208	1265A	2	*Pl, Ch*	0.269	0.184	0.919	*Pl*
ODP	208	1266C	2	*Pl, Ch*	0.237	0.174	0.35	*Pl*
ODP	208	1267A	2	*Pl, Ch*	0.237	0.212	0.213	*Pl*
IODP	342	U1403	1	*Pl, Ch, Zo*	0.115	0.137		
IODP	342	U1409 B	1	*Pl, Ch*	0.133	0.163		
IODP	342	U1409 C	1	*Pl, Pa, Th, Pl, Ch*	0.142	0.146		

Sedimentology and paleoenvironmental proxy records

Lithological classification for 46 cores and metrics of carbonate dissolution (represented by changes in weight percent of $CaCO_3$) for 36 cores was collected through literature review including shipboard data and published records (Panchuk et al 2008, Wade 2020, Supplemental Table 1.2). Benthic foraminiferal, bulk, and C_{org} $\delta^{13}C$ records were compiled for 39 cores, and a variety of oxygen and productivity proxies for were collected for 17 cores (Supplemental Table 1.3). These variables were compared to bioturbation intensity and burrow diameter datasets produced by this study.

Ichnofabric index

The extent of bioturbation in the sediments was identified semi-quantitatively via assignment of an ichnofabric index based on in-person measurement or high resolution image analysis of cores at the mm-scale (ii, Droser and Bottjer 1989, 1991). This involved visually analyzing and classifying the percentage of primary physical sedimentary structures such as laminations or bedding planes vs. the amount of mixing and/or visible trace fossils preserved in the sediments. If there is a complete lack of burrows and all primary sedimentary structures are preserved, 0% bioturbation is assumed and the assigned ichnofabric index is 1. An ii of 2 indicates up to 10% disturbance of the unmixed sediment fabric and the presence of discrete isolated trace fossils. An ii of 3 indicates disturbance of between 10-40% of the unmixed sediment fabric and some overlapping but generally isolated burrows. An ii of 4 indicates disturbance of between 40-60% of sediment, though some bedding is discernable, and burrows are overlapping. An ii of 5 indicates that bedding is completely disturbed, but burrows are still discrete in places and the fabric is completely mixed. An ii of 6 describes completely mixed or homogenized sedimentary fabric with no discernable discrete trace fossils. Within the ii 6 category, subcategories describe the amount of discrete trace fossils overprinted on the completely bioturbated sediment. However, bioturbation intensity is unchanged across all subcategories within an ii of 6 and 5, rather just a descriptive difference. Instead, identification of discrete trace fossils as a subcategory of ii 6 describes most recently emplaced discrete trace fossil on a background of completely homogenized sediments (Droser and Bottjer 1986, 1991).

Burrow identification and burrow diameter measurement

All discernable discrete trace fossils were identified and measured 5 cm above and below the PETM onset, defined by the onset of the negative $\delta^{13}C$ excursion or the benthic foraminiferal extinction horizon. In 14 cores, burrows were identified and diameters were measured in-person, while burrows from 32 other cores were measured from the IODP images utilizing Fiji ImageJ software (Schindelin et al. 2012; Schneider and Eliceiri, 2012). We identified five different types of trace fossils (Figure 1.1) in total from the 46 sites: *Planolites* is an unlined and unbranching cylindrical or near cylindrical burrow actively backfilled with sediments lithologically different from host matrix (Nicholson 1873; Pemberton & Frey 1982; Fillion & Pickerill 1990). Size varies greatly based on variety of organisms that can produce this trace. *Paleophycus* are lined, unbranched cylindrical burrows passively filled with lithologically similar material to host matrix (Hall 1847, Pemberton & Frey 1982; Fillion & Pickerill 1990). Again, a variety of organisms can produce this discrete trace fossil (Diez-Canseco et al. 2016). *Chondrites* are unlined dendritic, smooth-walled, asymmetrically branched burrows actively backfilled (Von Strenberg 1833; Crimes 1987). *Zoophycus* are small U and J-shaped spreiten-filled structures that are arranged in a helix-like pattern around a central shaft or tunnel (Massalongo 1855; Uchman 1995). As a feeding structure, a variety of annelids or arthropods are believed to be capable of creating this structure. *Thalassinoides* are branched cylindrical burrows interconnected by vertical shafts, made by crustaceans (Ehrenberg 1944; Uchman 1995).

Since the diversity of organisms as reflected by trace fossils, was relatively consistent across all sites, to assess any potential changes in the benthic community, we compared average and maximum burrow diameters in the 5 cm before and after the onset of the PETM. For this study, burrow diameters (cm) were separated into two time bins (Late Paleocene and PETM onset). Maximum burrow diameters were selected from each time bin and burrow diameters were averaged within the Late Paleocene and PETM onset bins. These data were mapped to investigate global patterns in trace fossil assemblages (Table 1, Savrda & Bottjer 1986; Smith et al. 2000).

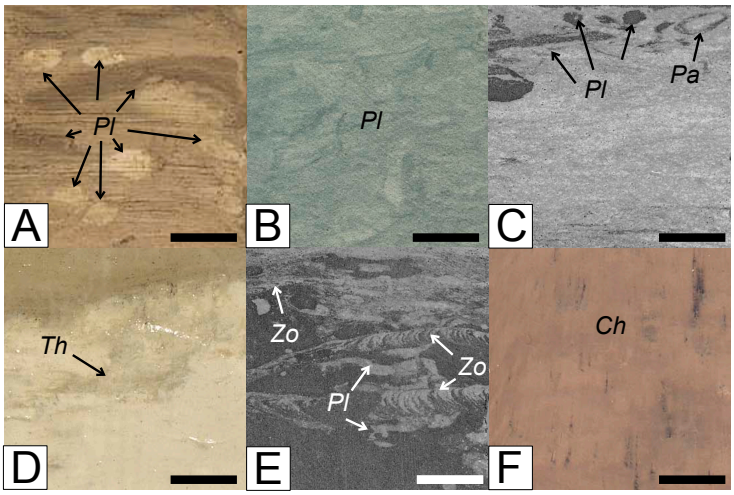

Figure 1.1 Discrete trace fossils from deep sea sediment cores spanning the Paleocene and Eocene. A. *Planolites* from ODP Site 1221D. B. Several *Planolites* from ODP Site 1260. C. *Planolites* and a *Paleophycus* as Site ODP 1001. D. *Thalassinoides* from site ODP 1210. E. *Planolites* and *Zoophycos* from site ODP 1001. F. Several *Chondrites*, identified as infilled by black sediment from site ODP 1262. All scale bars are 1 cm.

Results

PETM 'boundary types'

Through the analysis of sedimentological and ichnofabric information, we observed four patterns at the PETM onset that we classified as boundary types 1-4 (Figure 1.2). Boundary type 1 (BT1) is defined as no discernable change in bioturbation and sediment homogenization (ii of 5+) across the PETM onset. The 21 cores classified as BT1 (45.7 % of total) are found in all ocean basins except the Caribbean with paleodepths ranging from 1,000-4,600 m. The sediment composition of the cores varied, with 10 biogenic carbonate to clay sites, 8 biogenic carbonate dominant sites, 4 clay dominant sites, 1 porcellanite with clay site, and 1 siltstone dominant site.

Boundary type 2 (BT2) is defined as a late Paleocene bioturbated sedimentary unit (ii of 5+) completely separated by a distinct unconformity with an overlying bioturbated sediment unit encompassing the PETM onset, with 1 or more discrete trace fossil(s) piping through the unconformity but with that piping disturbing no more than 10% of the unconformity (ii of 2). In all 13 BT2 cores identified (30.4% of total), the underlying (late Paleocene) sediment is dominated by biogenic carbonate, the overlying (early Eocene) unit is clay, and the unconformity is due to dissolution (Bralower, T.J et al., 2002; Erbacher et al., 2004; Zachos et al. 2004). Six cores identified as BT2 were found at Walvis Ridge, 4 cores at Demerara Rise in the equatorial South Atlantic, and the remaining 3 were located at Shatsky Rise in the North Atlantic. The dissolution in the South Atlantic was most severe, with $CaCO_3$ wt% dropping to ~0% at Walvis Ridge

compared to ~85% at Shatsky Rise. *Thalassinoides* or *Planolites* were identified crossing the dissolution unconformity.

Boundary type 3 (BT3) is defined as an underlying (late Paleocene) bioturbated sedimentary unit (ii of 5+) separated by an unconformity with an overlying (early Eocene) bioturbated sedimentary unit (ii of 5+). No burrows cross-cut the unconformity. In the 9 cores classified as BT3 (19.5% of total) the unconformity is due to dissolution (Bralower et. al 1997; Erbacher et al., 2004; Zachos et al. 2004). Boundary type 3 is found in all ocean basins, though absent from the North Atlantic high latitudes. In 8 cores the underlying (late Paleocene) sediment is biogenic carbonate, and the overlying (early Eocene) unit is clay. The remaining core's underlying (late Paleocene) sediment was chalk and overlying (early Eocene) sediment shifted to clayey chalk. Boundary type 4 (BT4) is defined as a sharp transition from complete bioturbation (ii of 5+) to sustained cessation of bioturbation (ii of 1). The three BT4 cores (6.6% of total) are found in the South Equatorial Atlantic and Caribbean. The primary (late Paleocene) units are composed of chalk and limestone and the secondary (early Eocene) units of laminated claystone. Boundary types 2-4 all provide a descriptive framework for evaluating the extent of changes in bioturbation across the PETM onset.

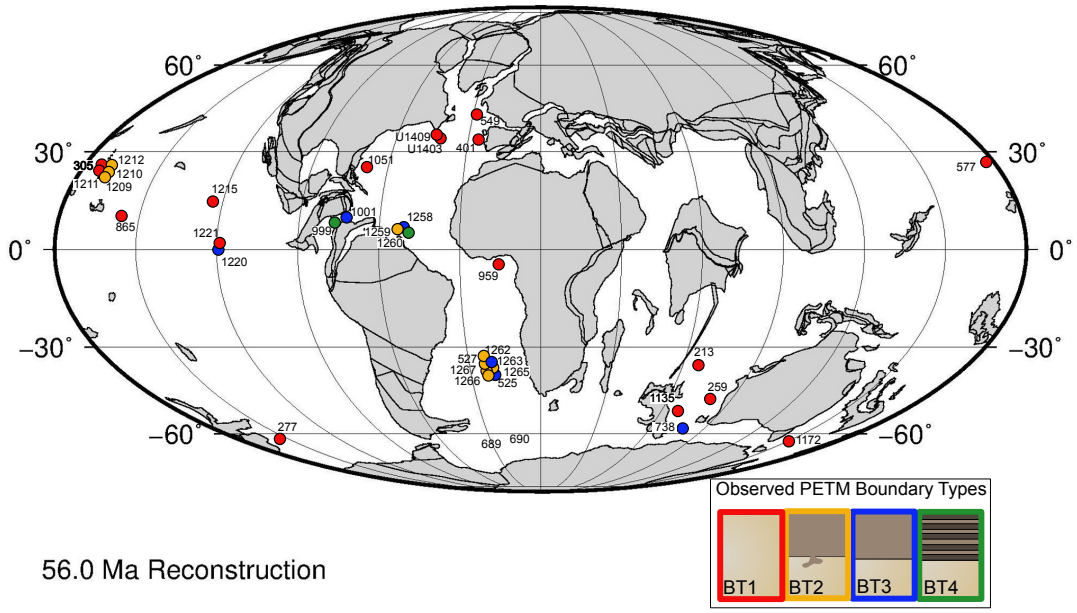

Figure 1.2: Map constructed utilizing ODSN Plate Reconstruction Service for 56Ma. All sites for the study are mapped and color coded based on boundary type, displayed in graphic. BT1 is red, BT2 is yellow, BT3 is blue and BT4 is green. All paleolatitudes used in study are found in Table 2.

Trace fossil assemblages

Discrete trace fossil assemblages varied globally across the 46 PETM sites, but diversity was low in the majority of cores. *Planolites* is the most abundant ichnotaxon appearing in all 46 cores, followed by *Paleophycus* (18 cores), *Chondrites* (15 cores), *Zoophycos* (3 cores), and *Thalassinoides* (2 cores). The trace fossil assemblage in the studied records can be assigned to the *Zoophycos* ichnofacies (MacEachern et al., 1999, 2012; Buatois and Mángano, 2011; Rodríguez-Tovar et al., 2015). Cores varied significantly in the number of discernable discrete trace fossils preserved, with the total number of burrows measured averaging ~6 in the 10 cm surrounding the PETM onset (min: 2, max: 35). In

46 cores, following the PETM onset, the maximum burrow diameter decreased 55.28% (0.220 cm) and the average burrow diameter decreased 51.73% (0.218) cm.

Ichnological analysis compared to other records

The three ichnological datasets collected here ('boundary types', average burrow diameter, and maximum differences across the PETM) were compared against each other and to paleo-latitude, paleo-depth, change in wt% $CaCO_3$ wt%, and $\delta^{13}C$ excursion magnitude (bulk and benthic) to determine if there were any correlations among these datasets (Table 1.2). The strongest correlation is between boundary type (BT1-4) and the difference in average burrow diameter across the PETM (R^2 0.797, 1.17e-16 p-value), followed by the correlation between boundary type and the difference in maximum burrow diameter (R^2 0.707, 4.85e-13 p-value). Boundary type has very weak positive correlations to the magnitude of the benthic $\delta^{13}C$ excursion (R^2 0.288, 0.0184 p-value), paleolatitude (R^2 0.195, 0.0021 p-value) and decrease in wt% $CaCO_3$ (R^2 0.144, 0.0116 p-value), and no correlation or significance to paleodepth (R^2 0.059, 0.104 p-value). Difference in maximum burrow diameter between the late Paleocene and PETM onset has weak positive correlation to the decrease in wt% $CaCO_3$ (R^2 0.301, 0.0115 p-value) and the magnitude of bulk $\delta^{13}C$ excursion (R^2 0.265, 0.0017 p-value), and no correlation or significance to the paleodepth (R^2 0.076, 0.0674 p-value), paleolatitude (R^2 0.007, 0.549 p-value) or magnitude of the benthic $\delta^{13}C$ excursion (R^2 0.033, 3.93E-1 p-value). Difference in average burrow diameter between the late Paleocene and PETM onset has weak correlation to the magnitude of bulk $\delta^{13}C$ excursion (R^2 0.238, 0.0248 p-value), and

no correlation to the paleodepth (R^2 0.043, 0.174 p-value), paleolatitude (R^2 0.007, 0.579 p-value), or magnitude of the benthic CIE (R^2 3.05E-05, 9.8E-0.1 p-value).

Table 1.2 Results of linear regression between variables in study. *=significant

Variable 1	Variable 2	r-squared	p-value
Boundary Type	Difference in average burrow diameter before after PETM onset	0.797	1.77E-16*
Boundary Type	Difference in maximum burrow diameter before after PETM onset	0.707	4.85E-13*
Difference in maximum burrow diameter before after PETM onset	CaCO3 difference at onset	0.301	0.00115*
Difference in maximum burrow diameter before after PETM onset	Magnitude of CIE: Bulk	0.265	0.0169*
Difference in average burrow diameter before after PETM onset	Magnitude of CIE: Bulk	0.238	0.0248*
Boundary Type	Magnitude of CIE: Benthic forams- Nuttallides truempyi	0.228	0.0184*
Boundary Type	paleolatitude	0.195	0.00212*
Boundary Type	CaCO3 difference at onset	0.144	0.0319*
Difference in maximum burrow diameter before after PETM onset	paleodepth	0.0757	0.0674
Boundary Type	paleodepth	0.059	0.104
Difference in average burrow diameter before after PETM onset	paleodepth	0.0426	0.174
Difference in maximum burrow diameter before after PETM onset	Magnitude of CIE: Benthic forams- Nuttallides truempyi	33	3.93E-01*
Boundary Type	Magnitude of CIE: Bulk	0.0304	4.38E-01*
Difference in average burrow diameter before after PETM onset	CaCO3 difference at onset	0.0209	0.43
Difference in maximum burrow diameter before after PETM onset	paleolatitude	0.00722	0.579
Difference in average burrow diameter before after PETM onset	paleolatitude	0.00489	0.648
Difference in average burrow diameter before after PETM onset	Magnitude of CIE: Benthic forams- Nuttallides truempyi	3.05E-05	9.80E-01*

Discussion

PETM and the ichnological record

There was a wide variety in ichnological responses following the onset of the PETM, highlighting the importance of local differences in environmental parameters affecting the macrobenthic realm. Oxygenation, sedimentation rate, and organic matter availability were likely the major limiting factors for bioturbating organisms in the deep sea (Wetzel, 1983; Giannetti and McCann, 2010; Wetzel, 2010; Uchman and Wetzel, 2011; Wetzel

and Uchman, 2012). We explore these limiting factors in relation to the described 'boundary types', ichnological diversity and size changes to evaluate any global or localized patterns.

Our boundary type classification cannot distinguish the exact timing between changes in bioturbation and the recovery of benthic mixing. However, boundary types (2-4) do record relative recovery patterns of the macrobenthic community, with BT2 returning previous patterns of mixing the quickest based on the observation that burrows can penetrate the preserved unconformity, while BT4 indicates the longest sustained cessation of bioturbation in order to allow preservation of multiple laminations.

Boundary Type 1

Changes in substrate composition and consistency can greatly impact ichnofabrics (Wetzel & Uchman 2012). When sediment shifts from carbonate dominated to clay dominated, the shear strength decreases, impacting the diversity of ichnogenera preserved and shortening the depth to which open burrows can penetrate (Savrda 2012). However, we found that BT1 occurred even with lithological transitions from biogenic carbonate to clay with a 40% weight loss in calcium carbonate (Panchuk et al., 2008). Hence the benthic community was able to thoroughly homogenize the sediments despite major lithological change, and there was no conclusive relationship between $CaCO_3$ wt. % loss and bioturbation cessation (Table 1.3, Nicolo 2010). Of course, changes in carbonate mass accumulation rate (MAR) would be a more accurate representation of dissolution intensity and duration throughout this interval, though the age control at all sites were not sufficient for comparison in this study. It appears that factors other than lithological

change were causing the cessation in bioturbation at other sites, or that the lithological changes at BT1 sites were sufficiently gradual that the benthic community was able to mix the sediments effectively under a variety of sedimentation rates (~0.3 cm/kyr in Pacific vs. 2.3 cm/kyr in the Southern Ocean; Bralower 2014; Wetzel, 2010). Given the ability for bioturbation to effectively erase primary sedimentary structures through homogenization, there is no conclusive evidence based on ichnological and sedimentological patterns from BT1 sites to determine whether bioturbation ceased for a short period of time at or after the PETM onset, if bioturbation intensity reduced, or if bioturbation patterns continued unchanged in intensity (Figure 1.3). For BT1 sites, the average decrease of burrow diameter was 0.16 cm between the late Paleocene and PETM onset; evidence that the infaunal organisms decreased in size in response to this environmental perturbation (Wetzel 2010). When compared to available proxy data (oxygen proxies: $\delta^{238}U_{CAU}$, $\delta^{53}Cr$, Mn and U enrichment factors, Ce/Ce*, presence of pyrite, presence of laminations; paleoproductivity proxies: Ba, benthic foraminifera assemblages), no global patterns emerge, while there is evidence of localized environmental factors such as decreases in oxygen availability (DSDP Sites 305 and 401), changes in organic matter availability (ODP Sites 865 and 1221), or evidence of both (ODP Sites 690, 738, 929, 1211).

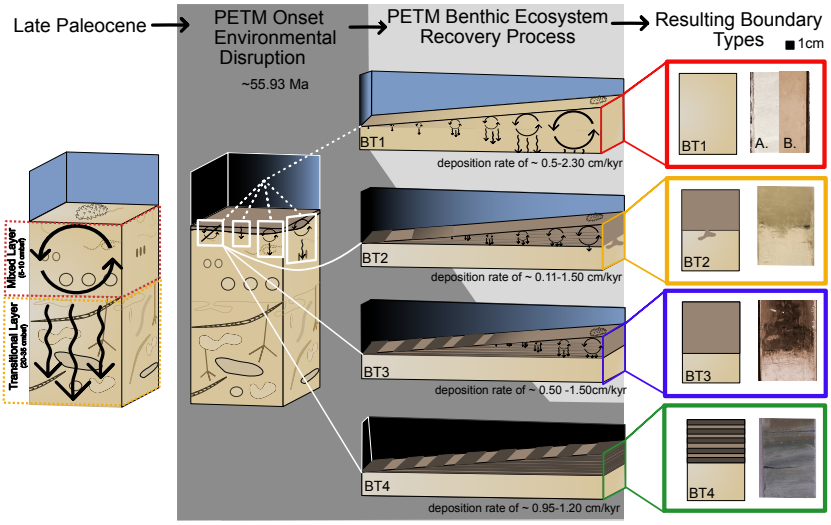

Figure 1.3 An illustration of hypothesized macrobenthic community's response to oceanic environmental conditions changing following the onset of the PETM. In the Late Paleocene sediment column, standard deep sea mixing conditions are shown with homogenization in the top 5-10 cm or "mixed layer", and heterogenous mixing of the "transitional layer" extending 20-35 cm below the mixed layer. The next column illustrates what occurs at the PETM onset. Dissolution occurred in carbonate-dominant sediments, causing varied amount of sediment 'burndown'. The macrobenthic organisms had a variety of responses ranging from cessation of bioturbation to normal patterns of bioturbation continuing. These options are show in the white boxes. One of four different boundary type results, depending on how quickly environmental conditions recovered. The grey background indicates the continued perturbation of environmental conditions (including changes in oxygen, temperature, pH, organic matter availability, or any combination of these factors) that would prevent the return of late Paleocene patterns of bioturbation. In boundary type one (BT1), bioturbation could have ceased, continued at normal levels, or anything in-between. But, patterns of bioturbation were able to completely homogenize the 5cm of sediment deposited, leaving an example of a completely homogenized sediment core of with clay or carbonate dominated lithology (A. ODP 738, B. ODP. 690). Boundary types 1-3 all preserve evidence of bioturbation ceasing. Their patterns of recovery are described: Boundary type two (BT2) bioturbation resumed the quickest, homogenized the unconformity layer, and one or a few transition layer burrows were able to penetrate the dissolution boundary. Boundary type three (BT3) represents a cessation of bioturbation, but sediments are completely bioturbated above and below the boundary. In Boundary type four (BT4), bioturbation ceases and does not return for at least 4 cm in which primary sedimentary features are preserved. Sedimentation rate ranges are taken from the representative cores investigated in study (Supplemental table 1.1).

Boundary Type 2

In boundary type 2, bioturbation ceased for enough time for a clay layer to form, preventing the majority of returning bioturbating organisms from homogenizing the boundary, yet some trace fossil makers were able to penetrate the dissolution unconformity. In 12 of the cores assigned as BT2, *Planolites* was the trace fossil found penetrating the unconformity in 11 cores while the remaining core's penetrative trace was *Thalassinoides*. In the 12 cores classified as BT2, the penetrative burrow(s) was an average 57.81% (0.20 cm) larger than the average burrow diameter of the PETM onset sediments, indicating that larger organisms penetrated the dissolution layer. As these burrows are larger than burrows within the underlying sediment into which they piped, one possibility is that they originated stratigraphically higher up the sediment core and represent a more recovered paleoenvironment (Savrda et al. 2012). Since color differentiation between the burrows and surrounding sediment matrix was insufficiently distinct to confidently determine the burrow's origin, we stratigraphically compared burrow depths through the core, and found that these larger penetrative burrow diameters were more similar to burrows measured ~5cm above the defined boundary. *Planolites* actively backfills its burrows, and these penetrative burrows' infill composition consists of clay, suggesting that a sufficient clay layer was built up in the sediments before the trace was made (MacEachern et al. 2007; Gingras et al. 2012). These lines of evidence suggest delayed penetrative burrower(s) crossing the dissolution boundary rather than a few bioturbating organisms actively creating trace fossils throughout the PETM onset as previously suggested (Bralower 2014).

Assuming that penetrative burrows represent a delayed recovery of larger burrowers, we consider possible explanations for a delayed return of typical deep-sea patterns of sediment homogenization after the cessation of bioturbation. These include substrate change, since it is more challenging for organisms to keep burrows open in clay due to its lower shear strength, and the thickness of the clay layer which might have prevented all but transitional layer organisms from penetrating the sediments (Savrda et. al 1984). However, both *Planolites* and *Thalassinoides* require softground sediment consistency for burrows to preserve (Wetzel and Uchman 1998), so sediment alteration did not prevent the responsible organisms from penetrating the clay-carbonate boundary. Due to the variety of organisms that can make the *Planolites* trace fossil, another possibility could be that a different group of organisms returned to the substrate following the PETM onset, and their burrowing capabilities were shallower when compared to previous trace makers' patterns (Pemberton & Frey 1982; Fillion & Pickerill 1990). With average burrow diameter decreasing by 61.95% (0.24cm) after the onset of the PETM, a combination of smaller trace fossil-makers combined with the increased physical challenges of burrowing in clay could have prevented most organisms present from mixing the boundary. Based on the relatively large size of the penetrative burrows, it appears that only the largest burrowing organisms had the physical capabilities to penetrate the dissolution unconformity (Sup. Table 2).

Boundary Type 3

In boundary type 3, bioturbation ceased long enough for a clay layer to form, preventing all remaining and/or returning bioturbating organisms from homogenizing the

boundary. When bioturbation returned, the organisms homogenized the overlying (early Eocene) sediment unit, but were unable to penetrate the underlying (late Paleocene) sedimentary unit. BT3 cores are found in South and equatorial Atlantic, Pacific and Caribbean Seaway. Following the onset of the PETM, average burrow diameters decrease by 68.21% (0.33 cm) and maximum burrow diameters decrease by 64.10% (0.29 cm). Assemblages remain *Planolites* dominant across the PETM onset, *Chondrites* increase in abundance following the onset of the PETM (Bromley & Ekdale 1984, Savarda 1992, Martin 2004). In 8 of 9 BT3 cores there is proxy data suggesting deoxygenation of bottom waters after the PETM onset (Chun et al., 2010; Post et al., 2016). If deoxygenation caused an extended cessation of bioturbation, coupled with 'burndown' carbonate dissolution, a significant clay layer should form. In 8 of 9 BT3 cores, there is evidence of increased export productivity following the PETM onset, though resolution is low, making it difficult to constrain the timing in the 5 cm investigated in this study (Ma et al. 2014). As nutrient availability and oxygen depletion gradually diminished and the benthic food supply recovered following the PETM onset, benthic macrofauna would have recolonized the uppermost sediment (mixed layer). However, it is likely that recovery was sufficiently slow that organic matter availability and perhaps oxygenation deeper in the sediments were insufficient for the establishment of a traditional tiered deep-sea trace maker community (Wetzel, 1991; Chester, 2000;).

Boundary Type 4

In boundary type 4, bioturbation ceased for thousands of years, allowing 4 cm at Site 999 and 12 cm at Sites 1260A and 1260B of laminated sediments to accumulate and

be preserved in the sedimentary record. The preservation of laminated sediments indicates a long-term drastic change in environmental conditions that forced extirpation of the macrobenthic community. Similar to BT2 and BT3, BT4 cores show massive $CaCO_3$ dissolution resulting in clay-rich laminations. No BT4 sites contain calcareous foraminifera in the clay beds, with the return of bioturbation paralleled by the return of poorly preserved and small benthic foraminifera, followed by distinct planktic foraminiferal fauna typical for the PETM (Bralower 1997; Erbacher et al. 2011). The three BT4 cores show the most extreme impacts from the PETM environmental perturbation. The presence of laminations in these sediments suggests sustained anoxia (Sluijs 2014), but it does not preclude other environmental changes such as acidification or changes in organic matter supply. Unfortunately, proxy records for oxygen independent of the presence of laminations, pH and nutrients are not available for these sites. The Caribbean core is linked to local volcanism based on preserved ash layers within the cores (Bralower 1997). At Caribbean Site 999, recovery is very gradual with small *Planolites* returning to the sediment, and complete homogenization not occurring for another 2 cm after the 4 cm-laminated interval, while the South Atlantic cores (Site 1260) do not recover in the 5 cm-interval following the PETM onset.

Global picture leads to localized patterns

The most distinct changes in bioturbation occurred in the Tropical Caribbean and Atlantic, where higher sedimentation rates (Site 999: 0.95 cm/kyr, Bralower 1997; Site 1260: 1.2 cm/kyr, Erbacher et al., 2004) dominated. The presence of extended laminations (classified as BT3) have been suggested as evidence for prolonged

diminished deep-water oxygenation (Bralower et al. 1997; Erbacher et al., 2004; Sluijs 2014). In an apparent contradiction, bottom waters at these sites have also been described as oligotrophic based on the lack of sedimentary organic matter, suggesting low organic carbon fluxes from surface waters, and the abundance of oligotrophic species (Bralower 2002, Mutterlose et al. 2007, Griffith et al. 2021). It is hence possible that the cessation of bioturbation was not caused by a lack of oxygen, but may be instead a drastic reduction in organic carbon arriving at the seafloor, potentially due to enhanced remineralization in the water column, which could have starved the benthic and infaunal community (Bralower 2002, Mutterlose et al. 2007, Griffith et al. 2021).

In the South Atlantic, there are meridional differences in bioturbation intensity, with bioturbation ceasing at all sites at Walvis Ridge, while the high latitude Southern Ocean sites show no cessation in bioturbation (Kelly et al. 2010, Bralower et al. 2014). In the Indian Ocean, ODP 738 is the only site to have evidence of bioturbation cessation across the PETM (BT3), as well as evidence of a suboxic seafloor argued as a consequence of an expanded oxygen minimum zone (OMZ, Sluijs et al. 2014). When compared to nearby site ODP 690 (BT1), site ODP 738 is only 3.16°N and 550m more shallow in depth.

In the Pacific we find 4 locations of bioturbation cessation, with three examples of BT1 at Shatsky Rise (ODP Sites 1209,1210, 1212), and BT2 in the equatorial Pacific (ODP Site 1220). In the equatorial Pacific, Site 1220, laminations appear delayed after the identified benthic foraminiferal extinction and a shift from carbonate to clay after the initial onset of the PETM, more consistent with peak barium values (Ma et al 2014).

Differences in patterns of bioturbation between the Atlantic and Pacific have been hypothesized to explain differences in carbonate preservation (Ridgwell 2007). However, hypotheses that bioturbation in the Pacific only ceased during peak dissolution and resumed vigorously afterward or continued with limited intensity throughout the interval (Bralower et al 2014; Bhattacharya et al. 2021) are inconsistent with the preservation of a sharp boundary minimally disturbed by later penetrative burrows (e.g. BT1). However, when comparing cores from Walvis Ridge and Shatsky Rise, it appears that at similar paleodepths depths (~2,600 mbsf), the patterns of 'boundary types' and burrow diameter size reduction are similar despite significant differences in carbonate burndown (Site 1209 ~7.5cm vs. Site 1263 ~23cm; Kelly et al. 2010, Bralower et al. 2014). With low sedimentation rates at both sites following the PETM onset (208: ~0.5cm/kyr Westerhold et al 2017; 198: ~0.3 cm/kry Bralower et al. 2014), the fact that a clay layer is still visible suggests that the eventual return of bioturbation took thousands of years, and when returned, was insufficient to thoroughly homogenize the sediments and erase the clay layer. The identified movement of pre-excursion single shell foraminiferal $\delta^{13}C$ record at Site 1209 suggests a very reduced mixed layer, perhaps only 3–5 cm (Zachos et al. 2003). Furthermore, bulk $\delta^{13}C$ values at Site 1210 decrease by ∼2‰ over a depth of only 3 cm, suggesting an extremely reduced mixed layer in the Pacific. The patterns of bioturbation recovery appear to be very similar among the BT2 of Shatsky Rise and Walvis Ridge, with similarly low sedimentation rates throughout the interval. Though differences in oxygen availability and organic matter availability might be the crucial difference between the two records. At Shatsky Rise, the sites remained oxic throughout the

interval while nutrient availability remained low (Ma et al 2014, Cu et al 2016). This may have supported sustained a shallower mixing depth throughout the whole interval, and caused a cessation due to starvation. Whereas, in the Atlantic, at Shatsky Rise, there is evidence of increased organic matter availability and evidence of reduced oxygen availability following the PETM onset. In this situation, the benthic community would have been suppressed due to a lack of oxygen, but due to increased nutrient availability, when the benthic community is able to return to the waters, they would be able to exploit the available nutrients in the sediments, and perhaps leading towards a greater mixing depth. Therefore, it is possible that bioturbation ceased for different amounts of times between the two locations in the ocean, but the 'boundary types' are not able to distinguish such differences.

Conclusions

Our analysis of ichnological features of deep-sea PETM sediments reveals major impacts on the macrobenthic community, with bioturbation ceasing at over 50% of sites globally. We also find a reduction in both average and maximum burrow size occurred globally, consistent with less hospitable environments for the benthic and infaunal community. However, we find no clear correlation between bioturbation cessation and patterns in PETM proxy records of the magnitude of the $\delta^{13}C$ excursion or decreases in deep-sea sedimentary wt% $CaCO_3$. Limited availability of proxy records for various paleoenvironmental changes (i.e. benthic organic matter availability, oxygen availability, pH), impedes attribution of changes in bioturbation to a single factor. Based on the lack

of correlation between ichnological features and either paleolatitude or paleodepth, it is likely that variable local controls determined the response of deep-sea bioturbators.

References

Alegret, L., Arreguín-Rodríguez, G. J., Trasvina-Moreno, C. A., & Thomas, E. (2021). Turnover and stability in the deep sea: Benthic foraminifera as tracers of Paleogene global change. *Global and Planetary Change*, *196*, 103372.

Alegret, L., Ortiz, S., & Molina, E. (2009). Extinction and recovery of benthic foraminifera across the Paleocene–Eocene Thermal Maximum at the Alamedilla section (Southern Spain). *Palaeogeography, Palaeoclimatology, Palaeoecology*, *279*(3-4), 186-200.

Alegret, L., Ortiz, S., Arenillas, I., & Molina, E. (2010). What happens when the ocean is overheated? The foraminiferal response across the Paleocene–Eocene Thermal Maximum at the Alamedilla section (Spain). *Bulletin*, *122*(9-10), 1616-1624.

Alegret, L., Reolid, M., & Pérez, M. V. (2018). Environmental instability during the latest Paleocene at Zumaia (Basque-Cantabric Basin): The bellwether of the Paleocene-Eocene Thermal Maximum. *Palaeogeography, Palaeoclimatology, Palaeoecology*, *497*, 186-200.

Bard, E., Arnold, M., Mangerud, J., Paterne, M., Labeyrie, L., Duprat, J., Duplessy, J. C. (1994). The North Atlantic atmosphere-sea surface 14C gradient during the Younger Dryas climatic event. *Earth and Planetary Science Letters*, *126*(4), 275-287.

Boudreau, B. P. (1998). Mean mixed depth of sediments: the wherefore and the why. *Limnology and Oceanography*, *43*(3), 524-526.

Bowen, G. J., Maibauer, B. J., Kraus, M. J., Röhl, U., Westerhold, T., Steimke, A., Clyde, W. C. (2015). Two massive, rapid releases of carbon during the onset of the Palaeocene–Eocene thermal maximum. *Nature Geoscience*, *8*(1), 44-47.

Bralower, T. J. (2002). Evidence of surface water oligotrophy during the Paleocene-Eocene thermal maximum: Nannofossil assemblage data from ocean drilling program Site 690, Maud rise, Weddell Sea. *Paleoceanography*, *17*(2), 13-1.

Bralower, T. J., Kelly, D. C., Gibbs, S., Farley, K., Eccles, L., Lindemann, T. L., & Smith, G. J. (2014). Impact of dissolution on the sedimentary record of the Paleocene–Eocene thermal maximum. *Earth and Planetary Science Letters*, *401*, 70-82.

Bralower, T. J., Kump, L. R., Self-Trail, J. M., Robinson, M. M., Lyons, S., Babila, T., Zachos, J. C. (2018). Evidence for shelf acidification during the onset of the Paleocene-Eocene thermal maximum. *Paleoceanography and Paleoclimatology*, *33*(12), 1408-1426.

Bromley, R. G., & Ekdale, A. A. (1984). Chondrites: a trace fossil indicator of anoxia in sediments. *Science*, *224*(4651), 872-874.

Bromley, R. G., & Ekdale, A. A. (1986). Composite ichnofabrics and tiering of burrows. *Geological magazine*, *123*(1), 59-65.

Bromley, R. G., & Ekdale, A. A. (1998). Ophiomorpha irregulaire (trace fossil): redescription from the Cretaceous of the Book Cliffs and Wasatch Plateau, Utah. *Journal of Paleontology*, *72*(4), 773-778.

Buatois, Luis A., and M. Gabriela Mángano. *Ichnology: Organism-substrate interactions in space and time*. Cambridge University Press, 2011.

Crouch, E. M., Dickens, G. R., Brinkhuis, H., Aubry, M. P., Hollis, C. J., Rogers, K. M., & Visscher, H. (2003). The Apectodinium acme and terrestrial discharge during the Paleocene–Eocene thermal maximum: new palynological, geochemical and calcareous nannoplankton observations at Tawanui, New Zealand. *Palaeogeography, Palaeoclimatology, Palaeoecology*, *194*(4), 387-403.

Dickens, G. R. (2011). Down the rabbit hole: Toward appropriate discussion of methane release from gas hydrate systems during the Paleocene-Eocene thermal maximum and other past hyperthermal events. *Climate of the Past*, *7*(3), 831-846.

Dickens, G. R., O'Neil, J. R., Rea, D. K., & Owen, R. M. (1995). Dissociation of oceanic methane hydrate as a cause of the carbon isotope excursion at the end of the Paleocene. *Paleoceanography*, *10*(6), 965-971.

Droser, M. L., & Bottjer, D. J. (1993). Trends and patterns of Phanerozoic ichnofabrics. *Annual Review of Earth and Planetary Sciences*, *21*(1), 205-225.

Droser, M. L., & Bottjer, D. J. 33. TRACE FOSSILS AND ICHNOFABRIC IN LEG 119 CORES.

Ekdale, A. A. (1977). Quantitative Paleoecological Aspects of Modern Marine Mollusk Distribution, Northeast Yucatan Coast, Mexico: Reef Biota.

Ekdale, A. A. (1980). Graphoglyptid burrows in modern deep-sea sediment. *Science*, *207*(4428), 304-306.

Ekdale, A. A. (1985). Paleoecology of the marine endobenthos. *Palaeogeography, Palaeoclimatology, Palaeoecology*, *50*(1), 63-81.

Ekdale, A. A., & Bromley, R. G. (1983). Trace fossils and ichnofabric in the Kjølby Gaard Marl, uppermost Cretaceous, Denmark. *Bulletin of the Geological Society of Denmark*, *31*(1), 107-11.

Ekdale, A. A., & Bromley, R. G. (1991). Analysis of composite ichnofabrics; an example in Uppermost Cretaceous chalk of Denmark. *Palaios*, *6*(3), 232-249.

Ekdale, A. A., Bromley, R. G., & Knaust, D. (2012). The ichnofabric concept. In *Developments in Sedimentology* (Vol. 64, pp. 139-155). Elsevier.

Fillion, D., Pickerill, R. K., & Harland, T. L. (1990). Influence de la diagenèse sur la production, la préservation et l'échantillonnage des ichnofossiles au sein des séries carbonatées: l'exemple du bassin intracratonique Ordovicien du Lac-St-Jean et de Chicoutimi (Québec). *Geobios*, *23*(4), 485-511.

Frieling, J., Gebhardt, H., Huber, M., Adekeye, O. A., Akande, S. O., Reichart, G. J., Sluijs, A. (2017). Extreme warmth and heat-stressed plankton in the tropics during the Paleocene-Eocene Thermal Maximum. *Science advances*, *3*(3), e1600891.

Frieling, J., Svensen, H. H., Planke, S., Cramwinckel, M. J., Selnes, H., & Sluijs, A. (2016). Thermogenic methane release as a cause for the long duration of the PETM. *Proceedings of the National Academy of Sciences*, *113*(43), 12059-12064.

Griffith, E. M., Fantle, M. S., Eisenhauer, A., Paytan, A., & Bullen, T. D. (2015). Effects of ocean acidification on the marine calcium isotope record at the Paleocene–Eocene Thermal Maximum. *Earth and Planetary Science Letters*, *419*, 81-92.

Griffith, E. M., Thomas, E., Lewis, A. R., Penman, D. E., Westerhold, T., & Winguth, A. M. (2021). Bentho-Pelagic Decoupling: The Marine Biological Carbon Pump During Eocene Hyperthermals. *Paleoceanography and Paleoclimatology*, *36*(3), e2020PA004053.

Gutjahr, M., Ridgwell, A., Sexton, P. F., Anagnostou, E., Pearson, P. N., Pälike, H., Foster, G. L. (2017). Very large release of mostly volcanic carbon during the Palaeocene–Eocene Thermal Maximum. *Nature*, *548*(7669), 573-577.

Hall, J. (1847). *Paleontology* (Vol. 1). Van Benthuysen. Hayek, L. A. C., Buzas, M. A., & Thomas, E. (2019). Identifying disruptions to the ecological balance of nature: a foraminiferal example across the initiation of the Paleocene–Eocene thermal maximum. *Paleobiology*, *45*(1), 98-113.

Heinze, M., & Ilyina, T. (2015). Ocean biogeochemistry in the warm climate of the late Paleocene. *Climate of the Past*, *11*(1), 63-79.

Hollis, C. J., Hines, B. R., Littler, K., Villasante-Marcos, V., Kulhanek, D. K., Strong, C. P., Phillips, A. (2015). The Paleocene–Eocene Thermal Maximum at DSDP Site 277, Campbell Plateau, southern Pacific Ocean. *Climate of the Past*, *11*(7), 1009-1025.

Jones, T. D., Lunt, D. J., Schmidt, D. N., Ridgwell, A., Sluijs, A., Valdes, P. J., & Maslin, M. (2013). Climate model and proxy data constraints on ocean warming across the Paleocene–Eocene Thermal Maximum. *Earth-Science Reviews*, *125*, 123-145.

Kelly, D. C., Nielsen, T. M., McCarren, H. K., Zachos, J. C., & Röhl, U. (2010). Spatiotemporal patterns of carbonate sedimentation in the South Atlantic: Implications for carbon cycling during the Paleocene–Eocene thermal maximum. *Palaeogeography, Palaeoclimatology, Palaeoecology*, *293*(1-2), 30-40.

Kennett, J. P., & Stott, L. D. (1991). Abrupt deep-sea warming, palaeoceanographic changes and benthic extinctions at the end of the Palaeocene. *Nature*, *353*(6341), 225-229.

Kirtland Turner, S., & Ridgwell, A. (2013). Recovering the true size of an Eocene hyperthermal from the marine sedimentary record. *Paleoceanography*, *28*(4), 700-712.

Koch, P. L., Zachos, J. C., & Gingerich, P. D. (1992). Correlation between isotope records in marine and continental carbon reservoirs near the Palaeocene/Eocene boundary. *Nature*, *358*(6384), 319-322.

Lobza, V., & Schieber, J. (1999). Biogenic sedimentary structures produced by worms in soupy, soft muds; observations from the Chattanooga Shale (Upper Devonian) and experiments. *Journal of Sedimentary Research*, *69*(5), 1041-1049.

MacEachern, J. A., & Pemberton, S. G. (1994). Ichnological aspects of incised-valley fill systems from the Viking Formation of the Western Canada Sedimentary Basin, Alberta, Canada.

MacEachern, J. A., Bann, K. L., Gingras, M. K., Zonneveld, J. P., Dashtgard, S. E., & Pemberton, S. G. (2012). The ichnofacies paradigm. In *Developments in sedimentology* (Vol. 64, pp. 103-138). Elsevier.

MacEachern, J. A., Pemberton, S. G., Gingras, M. K., Bann, K. L., & Dafoe, L. T. (2007). Uses of trace fossils in genetic stratigraphy. In *Trace fossils* (pp. 110-134). Elsevier.

Martin, K. D. (2004). A re-evaluation of the relationship between trace fossils and dysoxia. *Geological Society, London, Special Publications*, *228*(1), 141-156.
Massalongo, A. B. (1855). *Symmicta lichenum novorum vel minus cognitorum*. Antonelli.

Meissner, K. J., Bralower, T. J., Alexander, K., Jones, T. D., Sijp, W., & Ward, M. (2014). The Paleocene-Eocene thermal maximum: How much carbon is enough?. *Paleoceanography*, *29*(10), 946-963.

Mutterlose, J., Linnert, C., & Norris, R. (2007). Calcareous nannofossils from the Paleocene–Eocene Thermal Maximum of the equatorial Atlantic (ODP Site 1260B): evidence for tropical warming. *Marine Micropaleontology*, *65*(1-2), 13-31.

Nicholson, H. A. (1873). III. Contributions to the study of the errant Annelides of the older palæozoic rocks. *Proceedings of the Royal Society of London*, *21*(139-147), 288-290.

Nicolo, M. J., Dickens, G. R., & Hollis, C. J. (2010). South Pacific intermediate water oxygen depletion at the onset of the Paleocene-Eocene thermal maximum as depicted in New Zealand margin sections. *Paleoceanography*, *25*(4).

Pälike, C., Delaney, M. L., & Zachos, J. C. (2014). Deep-sea redox across the Paleocene-Eocene thermal maximum. *Geochemistry, Geophysics, Geosystems*, *15*(4), 1038-1053.

Panchuk, K., Ridgwell, A., & Kump, L. R. (2008). Sedimentary response to Paleocene-Eocene Thermal Maximum carbon release: A model-data comparison. *Geology*, *36*(4), 315-318.

Panchuk, K., Ridgwell, A., & Kump, L. R. (2008). Sedimentary response to Paleocene-Eocene Thermal Maximum carbon release: A model-data comparison. *Geology*, *36*(4), 315-318.

Party, S. S., Zachos, J. C., Kroon, D., & Blum, P. (2004). Leg 208 summary. In *Proc. ODP, Init. Repts* (Vol. 208, pp. 1-112).

Pemberton, G. S., Risk, M. J., & Buckley, D. E. (1976). Supershrimp: deep bioturbation in the Strait of Canso, Nova Scotia. *Science*, *192*(4241), 790-791.

Pemberton, S. G., & Frey, R. W. (1982). Trace fossil nomenclature and the Planolites-Palaeophycus dilemma. *Journal of Paleontology*, 843-881.

Pemberton, S. George, and Robert W. Frey. "Trace fossil nomenclature and the Planolites-Palaeophycus dilemma." *Journal of Paleontology* (1982): 843-881.

Penman, D. E., Hönisch, B., Zeebe, R. E., Thomas, E., & Zachos, J. C. (2014). Rapid and sustained surface ocean acidification during the Paleocene-Eocene Thermal Maximum. *Paleoceanography*, *29*(5), 357-369.

Raffi, I., & De Bernardi, B. (2008). Response of calcareous nannofossils to the Paleocene–Eocene Thermal Maximum: Observations on composition, preservation and calcification in sediments from ODP Site 1263 (Walvis Ridge—SW Atlantic). *Marine Micropaleontology*, *69*(2), 119-138.

Rodríguez-Tovar, F. J., & Uchman, A. (2010). Ichnofabric evidence for the lack of bottom anoxia during the lower Toarcian Oceanic Anoxic Event in the Fuente de la Vidriera section, Betic Cordillera, Spain. *Palaios*, *25*(9), 576-587.

Rodríguez-Tovar, F. J., Uchman, A., Alegret, L., & Molina, E. (2011). Impact of the Paleocene–Eocene Thermal Maximum on the macrobenthic community: Ichnological record from the Zumaia section, northern Spain. *Marine Geology*, *282*(3-4), 178-187.

Savrda, C. E. (2007). Taphonomy of trace fossils. In *Trace fossils* (pp. 92-109). Elsevier.

Savrda, C. E. (2012). Chalk and related deep-marine carbonates. In *Developments in Sedimentology* (Vol. 64, pp. 777-806). Elsevier.

Savrda, C. E. (2012). Chalk and related deep-marine carbonates. In *Developments in Sedimentology* (Vol. 64, pp. 777-806). Elsevier.

Savrda, C. E. (2016). Composite ichnofabrics: categorization based on number of ichnocoenoses and their temporal incongruence. *Palaios*, *31*(3), 92-96.

Savrda, C. E., & Bottjer, D. J. (1986). Trace-fossil model for reconstruction of paleo-oxygenation in bottom waters. *Geology*, *14*(1), 3-6.

Savrda, C. E., & Bottjer, D. J. (1987). The exaerobic zone, a new oxygen-deficient marine biofacies. *Nature*, *327*(6117), 54-56.

Savrda, C. E., & Bottjer, D. J. (1989). Trace-fossil model for reconstructing oxygenation histories of ancient marine bottom waters: application to Upper Cretaceous Niobrara Formation, Colorado. *Palaeogeography, Palaeoclimatology, Palaeoecology*, *74*(1-2), 49-74.

Savrda, C. E., & Bottjer, D. J. (1991). Oxygen-related biofacies in marine strata: an overview and update. *Geological Society, London, Special Publications*, *58*(1), 201-219.

Schieber, J. (2003). Simple gifts and buried treasures—implications of finding bioturbation and erosion surfaces in black shales. *The Sedimentary Record*, *1*(2), 4-8.
Schindelin, Johannes, et al. "Fiji: an open-source platform for biological-image analysis." *Nature methods* 9.7 (2012): 676-682.

Schneider, C. A., Rasband, W. S., & Eliceiri, K. W. (2012). NIH Image to ImageJ: 25 years of image analysis. *Nature methods*, *9*(7), 671-675.

Schneider, L. J., Bralower, T. J., Kump, L. R., & Patzkowsky, M. E. (2013). Calcareous nannoplankton ecology and community change across the Paleocene-Eocene Thermal Maximum. *Paleobiology*, *39*(4), 628-647.

Shaw, J. O., D'haenens, S., Thomas, E., Norris, R. D., Lyman, J. A., Bornemann, A., & Hull, P. M. (2021). Photosymbiosis in planktonic foraminifera across the Paleocene–Eocene thermal maximum. *Paleobiology*, 1-16.

Sluijs, A., Brinkhuis, H., Schouten, S., Bohaty, S. M., John, C. M., Zachos, J. C., ... & Dickens, G. R. (2007). Environmental precursors to rapid light carbon injection at the Palaeocene/Eocene boundary. *Nature*, *450*(7173), 1218-1221.
Sluijs, A., Schouten, S., Pagani, M., Woltering, M., Brinkhuis, H., Damsté, J. S. S., ... & Moran, K. (2006). Subtropical Arctic Ocean temperatures during the Palaeocene/Eocene thermal maximum. *Nature*, *441*(7093), 610-613.

Sluijs, A., Van Roij, L., Harrington, G. J., Schouten, S., Sessa, J. A., LeVay, L. J., ... & Slomp, C. P. (2014). Warming, euxinia and sea level rise during the Paleocene–Eocene Thermal Maximum on the Gulf Coastal Plain: implications for ocean oxygenation and nutrient cycling. *Climate of the Past*, *10*(4), 1421-1439.

Smith, C. R., Levin, L. A., Hoover, D. J., McMurtry, G., & Gage, J. D. (2000). Variations in bioturbation across the oxygen minimum zone in the northwest Arabian Sea. *Deep Sea Research Part II: Topical Studies in Oceanography*, *47*(1-2), 227-257.

Speijer, R., Scheibner, C., Stassen, P., & Morsi, A. M. M. (2012). Response of marine ecosystems to deep-time global warming: a synthesis of biotic patterns across the Paleocene-Eocene thermal maximum (PETM). *Austrian Journal of Earth Sciences*, *105*(1), 6-16.

Speijer, R., Scheibner, C., Stassen, P., & Morsi, A. M. M. (2012). Response of marine ecosystems to deep-time global warming: a synthesis of biotic patterns across the Paleocene-Eocene thermal maximum (PETM). *Austrian Journal of Earth Sciences*, *105*(1), 6-16.

Takeda, K., & Kaiho, K. (2007). Faunal turnovers in central Pacific benthic foraminifera during the Paleocene–Eocene thermal maximum. *Palaeogeography, Palaeoclimatology, Palaeoecology*, *251*(2), 175-197.

Tarhan, L. G. (2018). The early Paleozoic development of bioturbation—evolutionary and geobiological consequences. *Earth-Science Reviews*, *178*, 177-207.

Taylor, A. M., & Gawthorpe, R. L. (1993, January). Application of sequence stratigraphy and trace fossil analysis to reservoir description: examples from the Jurassic of the North Sea. In *Geological Society, London, Petroleum Geology Conference series* (Vol. 4, No. 1, pp. 317-335). Geological Society of London.

Taylor, A. M., & Goldring, R. (1993). Description and analysis of bioturbation and ichnofabric. *Journal of the Geological Society*, *150*(1), 141-148.

Teal, L. R., Bulling, M. T., Parker, E. R., & Solan, M. (2008). Global patterns of bioturbation intensity and mixed depth of marine soft sediments. *Aquatic Biology*, *2*(3), 207-218.

Teal, L. R., Parker, E. R., & Solan, M. (2010). Sediment mixed layer as a proxy for benthic ecosystem process and function. *Marine Ecology Progress Series*, *414*, 27-40.

Thomas, E. (2003). Extinction and food at the seafloor: A high-resolution benthic foraminiferal record across the Initial Eocene Thermal Maximum, Southern Ocean Site 690. *Special Papers-Geological Society of America*, 319-332.

Thomas, E., & Monechi, S. (2007). Cenozoic mass extinctions in the deep sea: What perturbs the largest habitat on Earth?. *SPECIAL PAPERS-GEOLOGICAL SOCIETY OF AMERICA*, *424*, 1.

Thomas, E., & Shackleton, N. J. (1996). The Paleocene-Eocene benthic foraminiferal extinction and stable isotope anomalies. *Geological Society, London, Special Publications*, *101*(1), 401-441.

Thomas, E., & Shackleton, N. J. (1996). The Paleocene-Eocene benthic foraminiferal extinction and stable isotope anomalies. *Geological Society, London, Special Publications*, *101*(1), 401-441.

Thomas, E., Zachos, J. C., & Bralower, T. J. (2000). Deep-sea environments on a warm earth: latest Paleocene-early Eocene.

Uchman, A. (1995). Tiering patterns of trace fossilsin the Palaeogene flysch deposits of the Carpathians, Poland. *Geobios*, *28*, 389-394.

Uchman, Alfred, and Andreas Wetzel. "Deep-sea ichnology: the relationships between depositional environment and endobenthic organisms." *Developments in Sedimentology*. Vol. 63. Elsevier, 2011. 517-556.

Wade, B. S., O'Neill, J. F., Phujareanchaiwon, C., Ali, I., Lyle, M., & Witkowski, J. (2020). Evolution of deep-sea sediments across the Paleocene-Eocene and Eocene-Oligocene boundaries. *Earth-Science Reviews*, 103403.

Webb, A. E., Leighton, L. R., Schellenberg, S. A., Landau, E. A., & Thomas, E. (2009). Impact of the Paleocene-Eocene thermal maximum on deep-ocean microbenthic community structure: Using rank-abundance curves to quantify paleoecological response. *Geology*, *37*(9), 783-786.

Westerhold, T., Röhl, U., Frederichs, T., Agnini, C., Raffi, I., Zachos, J. C., & Wilkens, R. H. (2017). Astronomical calibration of the Ypresian timescale: implications for seafloor spreading rates and the chaotic behavior of the solar system?. *Climate of the Past*, *13*(9), 1129-1152.

Wetzel, A. (1983). Biogenic structures in modern slope to deep-sea sediments in the Sulu Sea Basin (Philippines). *Palaeogeography, Palaeoclimatology, Palaeoecology*, *42*(3-4), 285-304.

Wetzel, A., & Uchman, A. (2012). Hemipelagic and pelagic basin plains. In *Developments in sedimentology* (Vol. 64, pp. 673-701). Elsevier.

Wetzel, Andreas. "Deep-sea ichnology: observations in modern sediments to interpret fossil counterparts." *Acta Geologica Polonica* 60.1 (2010): 125-138.

Winguth, A. M., Thomas, E., & Winguth, C. (2012). Global decline in ocean ventilation, oxygenation, and productivity during the Paleocene-Eocene Thermal Maximum: Implications for the benthic extinction. *Geology*, *40*(3), 263-266.

Witkowski, J., Harwood, D. M., Wade, B. S., & Bryłka, K. (2020). Rethinking the chronology of early Paleogene sediments in the western North Atlantic using diatom biostratigraphy. *Marine Geology*, *424*, 106168.

Yamaguchi, T., & Norris, R. D. (2012). Deep-sea ostracode turnovers through the Paleocene–Eocene thermal maximum in DSDP Site 401, Bay of Biscay, North Atlantic. *Marine Micropaleontology*, *86*, 32-44.

Zachos, J. C., Bohaty, S. M., John, C. M., McCarren, H., Kelly, D. C., & Nielsen, T. (2007). The Palaeocene–Eocene carbon isotope excursion: constraints from individual shell planktonic foraminifer records. *Philosophical Transactions of the Royal Society A: Mathematical, Physical and Engineering Sciences*, *365*(1856), 1829-1842.

Zachos, J. C., Röhl, U., Schellenberg, S. A., Sluijs, A., Hodell, D. A., Kelly, D. C., ... & Kroon, D. (2005). Rapid acidification of the ocean during the Paleocene-Eocene thermal maximum. *Science*, *308*(5728), 1611-1615.

Zeebe, R. E., & Zachos, J. C. (2007). Reversed deep-sea carbonate ion basin gradient during Paleocene-Eocene thermal maximum. *Paleoceanography*, *22*(3).

Zeebe, R. E., Zachos, J. C., & Dickens, G. R. (2009). Carbon dioxide forcing alone insufficient to explain Palaeocene–Eocene Thermal Maximum warming. *Nature Geoscience*, *2*(8), 576-580.

Zhou, X., Thomas, E., Rickaby, R. E., Winguth, A. M., & Lu, Z. (2014). I/Ca evidence for upper ocean deoxygenation during the PETM. *Paleoceanography*, *29*(10), 964-975.

CHAPTER 2: THE INFLUENCE OF BIOTURBATION ON BULK GEOCHEMICAL RECORDS ACROSS THE PALEOCENE-EOCENE THERMAL MAXIMUM

Abstract

The Paleocene-Eocene Thermal Maximum (PETM, ~56 Ma) was an abrupt period of greenhouse warming, during which thousands of gigatons of isotopically depleted carbon were added to the atmosphere over the span of a few thousand years, leading to a global negative carbon isotope excursion (CIE) and carbonate dissolution. Deep-sea sediment cores are key sources of information for these changes in climate and global carbon cycling; however, their geological record is subject to alteration through animal burrowing, or bioturbation, within the sediments after deposition. Across the PETM, differences in bioturbation intensity between ocean sites can provide unique insight into the severity of impacts on the benthic environment while physically mixing the sediment, influencing carbonate dissolution and possibly obscuring various geochemical indicators including the shape of the CIE. Here, we determine the ichnofabric index from three ocean drilling sites across the Pacific, which reveals significant spatial differences in the intensity of bioturbation. Next, we employ a novel burrow-specific sampling technique to assess the potential impact of sampling burrows on bulk carbonate stable isotope ($\delta^{13}C$ and $\delta^{18}O$) records from these sites. Our analyses demonstrate that sampling preserved discrete trace fossils can impact geochemical records at all degrees of bioturbation

intensity, with the greatest differences associated with sampling discrete trace fossils near intervals of extreme climatic changes. We suggest avoidance of sampling discrete burrows for the production of geochemical records across intervals of rapid climatic changes.

Introduction

Deep-sea sediments are important archives of past climate change events. The Paleocene-Eocene Thermal Maximum (PETM; Zeebe & Lourens 2019) is widely considered the best paleo-analog for future greenhouse gas-driven warming. During the PETM, global temperature rose between 5–8 °C (Kennett & Stott, 1991; Dunkley Jones et al., 2013) and a global negative carbon isotope excursion (CIE) of <2‰ over 20 kyr indicates a rapid injection or injections of isotopically depleted carbon into the ocean and/or atmosphere (Bralower et al., 1997; Kennett & Stott, 1991; McInerney and Wing, 2011). Following the rapid onset, the PETM had an extended recovery period relative to the onset, resulting in a total duration of ~170 kyr (Farley & Eltgroth, 2003; McInerney & Wing, 2011; Röhl et al., 2007; Zeebe & Lourens, 2019).

The deep-sea benthic environment changed dramatically across the PETM, with a deep sea benthic foraminifera extinction (e.g., Thomas, 1990, 1998, 2003, 2007), benthic ocean acidification (e.g. Meissner, et al., 2014; Ridgwell, 2007a; Zachos et al., 2005), reduced oxygen content (Pälike et al. 2014, Chang et al. 2018, Dickson et al 2012) and hypothesized cessations of sediment mixing by organisms at some locations (Ridgwell, 2007).

An expected consequence of this massive environmental perturbation, which altered sedimentation rates, global patterns of carbonate dissolution, and sediment mixing intensity, would be a disruption to the expected age-depth relationship within deep-sea sediment cores (e.g., Kelly et al., 1996; Ridgwell, 2007; Bralower et al., 2014). This sediment mixing, or bioturbation, is performed by organisms at or below the sediment-water interface and resulting in the homogenization of surface and previously deposited sediments as well as piping newer deposited sediment to greater depths (Darwin 1892; Guinasso & Schink 1975; Aller, 1982; Droser & Bottjer 1989; Crimes & Droser 1992, Meysman et al., 2006).

In the deep sea, sedimentation rates are very slow, averaging ~1.50 cm/kyr (Lyle, 2016), while sediment homogenization averages ~10cm below the water-sediment interface (Bard, 1994; Boudreau 1994; Teal et al., 2008, 2010). In the absence of extreme environmental factors (i.e. changes in oxygen availability, sedimentation rate, substrate consistency, salinity, nutrient availability), bioturbation reworks the primary sedimentary structures and shallow burrows (Ekdale et al., 1984, Tarhan 2018).

However, even in completely bioturbated deep-sea sediments, preserved discrete trace fossils that dominate the fossilized ichnofabric called ‘elite faunas’ include *Chondrites, Planolites, Paleophycus, Zoophycos,* and *Thalassinoides* (Ekdale 1977; Ekdale 1980; Bromely 1990; Droser and Bottjer 1991; Bromely 1996). Preserved burrows are largely biased towards the structures produced by deeper-burrowing infauna and are preserved in the “transition layer” which can extend from 10cm-2m below the sediment-water interface, where mixing shifts from homogenization to preserved

structures (Pemberton et al., 1976, Ekdale et al., 1984; Bromley, 1996, Lobza and Schieber, 1999; Schieber, 2003; Tarhan 2018).

Often suggested as the mechanism for extreme outlying ages identified from populations of individual foraminifera specimens in a single stratigraphic layer, the discrete fossils' impact on bulk sediment geochemical records is still debated (Kennett & Stott,1991; Löwemark & Werner, 2001; Löwemark & Grootes, 2004; Küssner et al., 2018; Lougheed et al. 2018; Dolman et al. 2021). While the effect of bioturbation on the preservation of proxy signals has been examined extensively through physical modeling of sediment mixing (e.g. Berger & Heath 1968; Berger et al., 1977; Bard et al., 1987; Trauth, 1998, 2013; Hull et al., 2011; Steiner et al., 2016; Kirtland Turner et al., 2017, Hulse et al., 2018, Kanzaki et al 2021), paleontological and geochemical reconstruction of the depth-dependent combination of homogenization of the mixed layer and later overprinting by deeper-burrowing infauna should lead to better understanding of taphonomic biases in these records. Preservation of discrete trace fossils provides the opportunity to determine the impact on bulk geochemical records of the deeper-burrowing infauna.

The PETM was selected as a case study due to the major changes in the benthic environment and hypothesized cessations in bioturbation in different ocean basins, with implications for both carbonate dissolution and the preservation of proxy signals. Bioturbation, by mixing carbonate particles from depth to the sediment surface provides a local buffering service and prevents complete dissolution. In the absence of bioturbation, sedimentary clay layers will more readily form in response to lower deep ocean

saturation state (Ridgwell 2007). If bioturbation was reduced (or ceased altogether) this also provides an opportunity to visually evaluate the movement of sediment as deeper-burrowing infauna later returned. In the absence of obvious changes in lithology with depth, sediment homogenization can obscure the traces of elite burrowers. The gradual reemergence of the mixed layer should illuminate the relationship between shallow sediment homogenization and deep mixing and the influence of these different mixing styles on geochemical records. Here we classify the bioturbation intensity from Pacific Ocean Drilling Program (ODP) drilling Sites 1209, 1220, and 1221 and employ a novel burrow-specific sampling technique across the PETM to assess the impact of elite bioturbating organisms on bulk carbonate stable isotope ($\delta^{13}C$ and $\delta^{18}O$) records from these sites.

Materials

Three cores spanning the Paleocene-Eocene Thermal Maximum CIE were selected for this study based on their excellent preservation of discrete trace fossils throughout the PETM interval and availability of material: Ocean Drilling Project (ODP) Leg 198 Site 1209C, and ODP Leg 199 Sites 1220B and 1221D.

Hole 1209C (32°19.6104′N, 158°10.6824′E) was drilled at Shatsky Rise in the North Pacific, at a water depth of 2387 m. Over the interval investigated (197.500-196.700 mbsf), the PETM was identified slanted at the depth of 197.290-197.300 mbsf as a dramatic sedimentological change from white nannofossil ooze to a brown nannofossil ooze, with the boundary disturbed during coring and splitting (Bralower 2001). The depth

of the PETM was further constrained by benthic isotope records (Bralower 2001, Westerhold 2006).

Holes 1220B (10°10.600′N, 142°45.503′W) and 1221D (12°01.999′N, 143°41.572′W) were both drilled in the equatorial Pacific Ocean at water depths of 5218 m and 5175 m, respectively. Both sites have similar distinctive brown, pink, black, and dark brown layering of clays and chalk that have been correlated across the PETM on a cm-scale though drilled 206 km apart (Lyle et al 2001). For Hole 1220B, we evaluate the interval from 199.850-198.910 mbsf; the PETM was identified at 199.68 mbsf by the last occurrence of *Gavelinella beccariiformis* (Lyle 2001) and later confirmed by the benthic foraminiferal $\delta^{13}C$ excursion (Nunes and Norris, 2005, 2006). For Hole 1220D, we evaluate the interval from 153.000 to 151.780 mbsf, with the PETM identified at 152.690 mbsf based on a peak in magnetic susceptibility and identification of the benthic foraminifera extinction event with the disappearance of *A. velascoensis*, *Gyroidinoides globosus*, and *G. beccariiformis* (Lyle 2001).

Methods

Bioturbation intensity commonly varies widely across temporal and spatial scales due to its sensitivity to environmental factors (McIlroy, 2007). For this reason, we assess bioturbation in a highly resolved stratigraphic context across each of the three PETM sections. We analyzed all cores in-person at least every cm, but recorded changes at the mm-scale when necessary to fully capture sedimentological and ichnological variations.

We identified and measured the burrow diameter of all discrete trace fossils from each studied interval.

Three 'elite fauna' trace fossils were identified in the three studied sections. *Planolites* is an unlined, unbranching, actively backfilled cylindrical burrows actively backfilled with sediments different from primary sediments trace, that can vary greatly in size and organism that produces the trace (Nicholson 1873; Pemberton & Frey 1982; Fillion & Pickerill 1990). *Paleophycus* are unbranched burrows passively filled with litholigically similar material to host matrix that are lined that can vary greatly in size and organism that produces the trace (Hall 1847, Pemberton & Frey 1982; Fillion & Pickerill 1990; Diez-Canseco et al. 2016). *Chondrites* are actively backfilled asymmetrically branched unlined and dendritic burrows (Von Strenberg 1833; Crimes 1987).
Through the visual analyzation and classification of the percentage of primary physical sedimentary structures vs. the amount of mixing and/or visible trace fossils preserved via assignment of an ichnofabric index (ii, Figure 2.1, Droser and Bottjer 1989, 1991), we are able to semi-quantitatively identify the extent of bioturbation in these cores. The sediment is assigned an ii of 1 if 0% bioturbation is assumed, and only primary sedimentary structures are present. An ii of 2 denotes up to 10% disturbance of the unmixed sediment fabric with the presence of discrete isolated trace fossils. An ii of 3 commonly includes some overlapping but generally isolated burrows, with between 10-40% of the unmixed sediment fabric, whereas an ii of 4 has burrows are overlapping with disturbance of between 40-60% of sediment, and only some bedding is discernable. The remaining ii of 5, 6, and the various subcategories of 6 indicate completely disturbed

bedding and complete bioturbation, with variable amounts of discernable discrete trace fossils. An ii of 5 contains the most discrete trace fossils preserved, with no primary bedding visible in the sediment, while all ii of 6 contain evidence of background of completely homogenized sediments Droser and Bottjer 1986, 1991). However, bioturbation intensity is unchanged across all subcategories within an ii of 6 and 5, rather just a descriptive difference (Droser and Bottjer 1986, 1991).

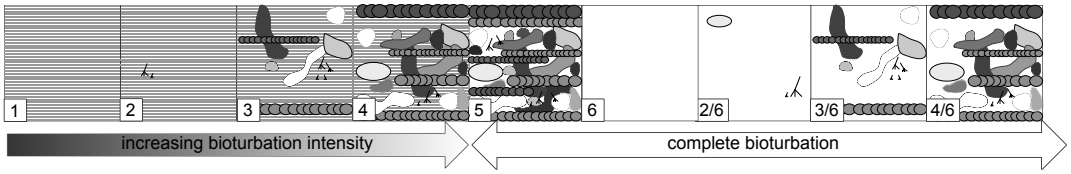

Figure 2.1 Deep sea ichnofabric index adapted from Droser and Bottjer 1991. A scale to analyze and classifying the percentage of primary physical sedimentary structures vs. the amount of mixing and/or visible trace fossils preserved in the sediments.

Geochemical sampling protocol and novel burrow-specific sampling technique

In each of the three sites spanning the PETM (previously identified by magnetic susceptibility, biostratigraphic, and benthic isotopic records) we took two 'toothpick'-sized bulk sediment samples from each stratigraphic interval where a burrow was identified: one inside the burrow, and one directly adjacent to the burrow. Samples were taken only from *Planolites* and *Paleophycus* burrows because *Chondrites* burrows were too small to obtain a sample. Additionally, bulk sediment samples were taken at 5cm intervals one centimeter from the available edge of the core and regardless of the occurrence of burrows. We refer to these as 'standard samples.'

All samples were oven dried and homogenized by mortar and pestle, and ~45-200μg of bulk carbonate sediment was analyzed for stable carbon and oxygen isotopes ($\delta^{13}C$ and $\delta^{18}O$) using a ThermoFisher Delta V (UC Riverside) stable isotope mass spectrometer coupled to a Keil IV carbonate device. Results are expressed relative to the Vienna Pee Dee Belemnite standard. The long-term $\delta^{13}C$ and $\delta^{18}O$ reproducibility of carbonate standards run concurrently with samples was < ±0.03 ‰ for $\delta^{13}C$ and <± 0.07‰ for $\delta^{18}O$ (±1 standard deviation). Duplicates were run when sample size and carbonate content allowed. All plotted error bars are based on the standard deviation of duplicate measurements. Calcium carbonate weight percent for each 'standard sample' was estimated via regression of the sample weight and total CO_2 yielded following acidification for all pure carbonate standards.

Results

1209C pre-PETM

We define the PETM onset at 197.295 mbsf based on dramatic lithological changes in carbonate content and preservation, and confirmed by the onset of the benthic foraminifera carbon isotope excursion (Figure 2.2, Bralower 2001, Westerhold 2006). The $\delta^{13}C$ of pre-PETM bulk standard samples from 197.500 to 197.290 mbsf averages 2.799‰ and $\delta^{18}O$ averages -0.793‰. The estimated $CaCO_3$ averages 96.68%. The ichnofabric index is 2/6, with rare *Planolites* burrows measuring an average of 0.441 cm (0.681 max, 0.171min). Paired in-and-out-of-burrow measurements at 197.47 mbsf yield in-burrow $\delta^{13}C$ 0.378‰ lower than the out-of-burrow value, but $\delta^{18}O$ values that are

identical within standard of error from duplication. Immediately below the PETM onset at 197.3 mbsf, paired in-and-out-of-burrow measurements are significantly offset. $\delta^{13}C$ is 0.853‰ lower in the out-of-burrow sample compared to the in-burrow sample, such that the in-burrow sample is consistent with the pre-PETM value obtained from the standard bulk sample at this depth, while the out-of-burrow sample registers the onset of the PETM $\delta^{13}C$ excursion. However, the reverse is true for $\delta^{18}O$ – the in-burrow $\delta^{18}O$ value is lower than the out-of-burrow value.

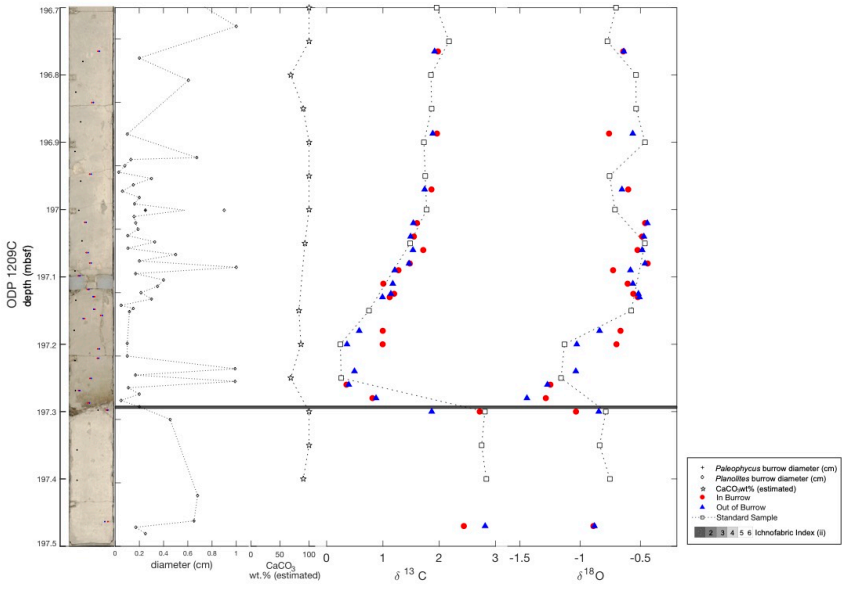

Figure 2.2 Image of core 1209C (taken at repository) with sites of sample indicated (red circle for in burrow, blue circle for out of burrow, and black square for standard sample). The ichnofabric index is represented as a color gradient behind the panel, with darkest grey representative as 1 or no mixing, and white representing 5,6, and all the subcategories of 6, as they are descriptive terms for completely mixed. The ichnofabric index is plotted against depth (mbsf). All measured discrete trace fossil diameters in black diamonds (*Planolities*) and black ∗ (*Chondrites*), with the black dotted line representing average burrow diameter all plotted vs. meters below the seafloor (mbsf). Estimated $CaCO_3$ wt. % plotted in black stars with black dotted line vs. mbsf. Bulk carbonate $\delta^{13}C$ and $\delta^{18}O$ from inside burrows (red circles), outside burrows (blue triangles), standard samples (black squares with grey line) plotted vs. mbsf.

PETM onset and peak of excursion

The peak (minimum) of the PETM $\delta^{13}C$ excursion extends from 197.290 to 197.180 mbsf in standard bulk samples. $\delta^{18}O$ is also lowest in this interval and the estimated $CaCO_3$ is reduced to ~77.00%. Bioturbation ceases coincident with the PETM onset at 197.295 mbsf and a thin clay layer is visible. No visible burrows penetrated the sediment below this thin clay layer. For the remainder of the PETM body, sediments are completely homogenized (ii of 2/6) with rare discrete *Planolites* averaging 0.323 cm in diameter (0.990 max, 0.049 min). Five in-and-out-of-burrow pairs were sampled from 197.290 to 197.180 mbsf across the PETM onset and peak, though carbonate content was insufficient for a measurement from one in-burrow sample. Two in-burrow samples at 197.280 mbsf and 197.260 mbsf show a lower $\delta^{13}C$ but higher or indistinguishable $\delta^{18}O$ compared to the corresponding out-of-burrow samples. At 197.200 mbsf and 197.18 the in-burrow samples are higher in both $\delta^{13}C$ and $\delta^{18}O$ compared to the out-of-burrow samples by ~0.052‰.

Recovery

Based on the 'standard' bulk $\delta^{13}C$ record, values begin increasing from ~197.180 mbsf to the top of the measured interval at 196.7 mbsf, though they never reach pre-PETM values. The estimated wt% $CaCO_3$ generally increases throughout this interval, averaging 92.65%, and sediments are completely homogenized (ii of 6 and 2/6), with rare *Planolities* with an average diameter of 0.250cm (max: 1 cm, min: 0.03). Eleven in-and-out-of-burrow pairs were sampled. $\delta^{13}C$ and $\delta^{18}O$ measurements for in-and-out-of-burrow pairs are within error of each other at two depths (197.08 and 196.765). However, the

difference between in-and-out-of-burrow measurements is generally minor in comparison to the pair sampled at the PETM onset (197.300 mbsf) and the two pairs sampled within the PETM body at 197.200 and 197.180 mbsf.

ODP Hole 1220 (Figure 2.3)

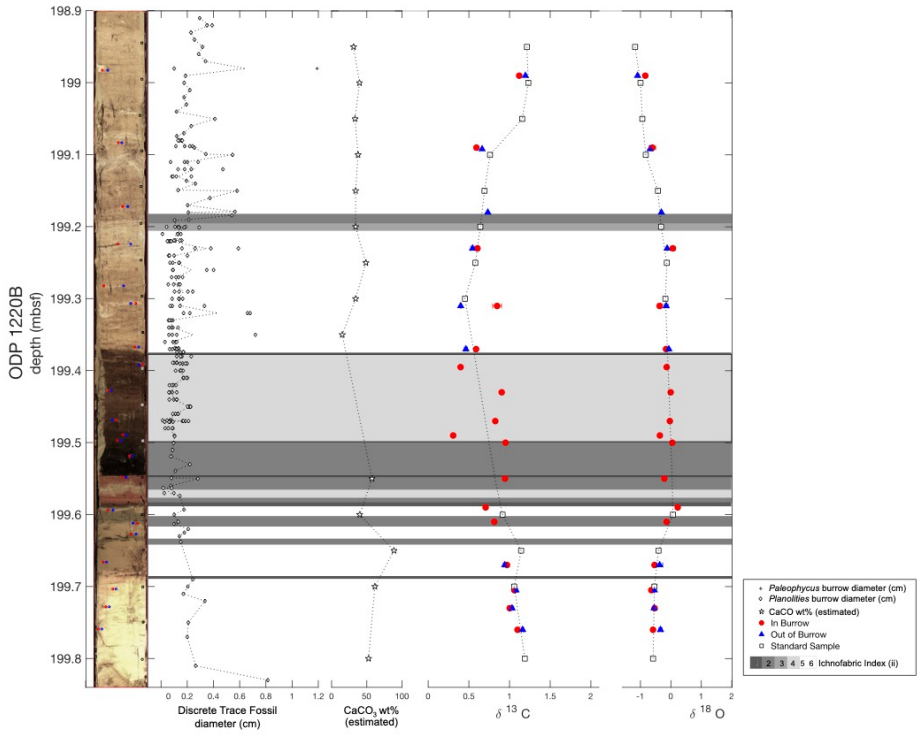

Figure 2.3: Image of core 1220 (from IODP Image Library) with sites of sample indicated (red circle for in burrow, blue circle for out of burrow, and black or white square for standard sample). The ichnofabric index is represented as a color gradient behind the panel, with darkest grey representative as 1 or no mixing, and white representing 5,6, and all the subcategories of 6, as they are descriptive terms for completely mixed. The ichnofabric index is plotted against depth (mbsf). All measured discrete trace fossil diameters in black diamonds (*Planolities*) and black crosses (*Paleophycus*), with the black dotted line representing average burrow diameter all plotted vs. meters below the seafloor (mbsf). Estimated $CaCO_3$ wt. % plotted in black stars with black dotted line vs. mbsf. Bulk carbonate $\delta^{13}C$ and $\delta^{18}O$ from inside burrows (red circles), outside burrows (blue triangles)and standard samples (black squares with grey line) plotted vs. mbsf.

Pre-PETM

We define the PETM onset based on the reported depth of the benthic foraminiferal extinction at 199.68 mbsf (Lyle et al. 2001). In the evaluated pre-PETM interval between 199.850 to 199.688 mbsf, $\delta^{13}C$ of 'standard' bulk samples averages 1.123‰ and $\delta^{18}O$ averages -0.564 ‰. Estimated $CaCO_3$ averages 56.96%. Sediment was assigned an ii of 2/6, indicating complete homogenization with rare discrete *Planolities* whose diameters average 0.30 cm (min: 0.01, max: 0.815). We sampled three in-and-out-of-burrow pairs from pre-PETM sediments. $\delta^{13}C$ and $\delta^{18}O$ are very similar for each of these pairs. Samples at 199.76 mbsf are slightly more depleted inside the burrow (0.063‰ lower $\delta^{13}C$ and 0.247‰ lower $\delta^{18}O$) while the other two pairs at 199.73 and 199.705 mbsf are identical within analytical error.

PETM onset and missing peak of excursion

The benthic foraminiferal extinction indicates the PETM onset occurs at 199.680 mbsf, but in our isotopic records, there is no clear excursion at this depth. Based on previously published benthic foraminifera isotopic records (Nunes and Norris 2005, 2006), the onset and peak (minimum) of the CIE occurs between 199.680 and 199.350 mbsf. However, 'standard' bulk sample $\delta^{13}C$ and $\delta^{18}O$ between 199.650-199.550 mbsf are consistent with pre-excursion values, and the estimated $CaCO_3$ averages 61.92%. Between 199.550 and 199.350 mbsf, 'standard' bulk samples contained insufficient carbonate for isotopic analysis. The interval between 199.688 to 199.470 mbsf also coincides with lithological changes from red to black to brown clay, followed by a shift to brown calcareous chalk for the reminder of the interval. Bioturbation intensity varies

significantly between an ii of 1 to 6, and average burrow diameter decreases to 0.127 cm (min 0.012, max 0.720). Bioturbation first ceases (ii=1) for 0.5 cm (199.688-199.683 mbsf), immediately below the identified benthic foraminiferal extinction event at 199.68 mbsf but subsequently recovers to an ii of 6. Throughout the interval, bioturbation intensity shifts dramatically between complete homogenization and preserved laminations with three additional discrete depth intervals with ii of 1: 199.593-199.578 mbsf, 199.549-199.540 mbsf, and 199.386-199.381 mbsf. Of the two in-and-out-of-burrow sample pairs with sufficient carbonate for analysis in this interval, the pair at 199.670 mbsf has indistinguishable $\delta^{13}C$ and $\delta^{18}O$, while the pair at 199.370 has offsets of 0.126 in $\delta^{13}C$ and 0.095 in $\delta^{18}O$. Pairs of in-and-out-of-burrow samples between 199.6 to 199.4 mbsf only yielded $\delta^{13}C$ and $\delta^{18}O$ measurements from the in-burrow sample. These generally show intermediate $\delta^{13}C$ values and pre-event or recovery $\delta^{18}O$ values, though the burrow sampled at ~199.50 mbsf has low $\delta^{13}C$, but pre-event or recovery $\delta^{18}O$.

Recovery

Though there is no distinct CIE onset in the produced records, based on previously published benthic isotopic records (Nunes and Norris 2005, 2006) $\delta^{13}C$ values increase from the minimum across the interval of 199.350-198.910. Across this interval, the $\delta^{13}C$ of the 'standard' bulk samples increases from a minimum of 0.452‰ at 199.300 to greater than 1.0‰ by 199.050 mbsf with estimated wt% $CaCO_3$ averaging 34.19%. The sediment consists of brown calcareous chalk, and is thoroughly bioturbated (ii of 5+) except between 199.201 to 199.800 mbsf, where bioturbation intensity is reduced (ii of 3

and 2). In-and-out-of-burrow pairs yield similar $\delta^{13}C$ and $\delta^{18}O$ values, with an exception at 199.31 mbsf, where the $\delta^{13}C$ of the out-of-burrow sample is 0.477‰ lower and the $\delta^{18}O$ is 0.214‰ higher compared to the in-burrow sample.

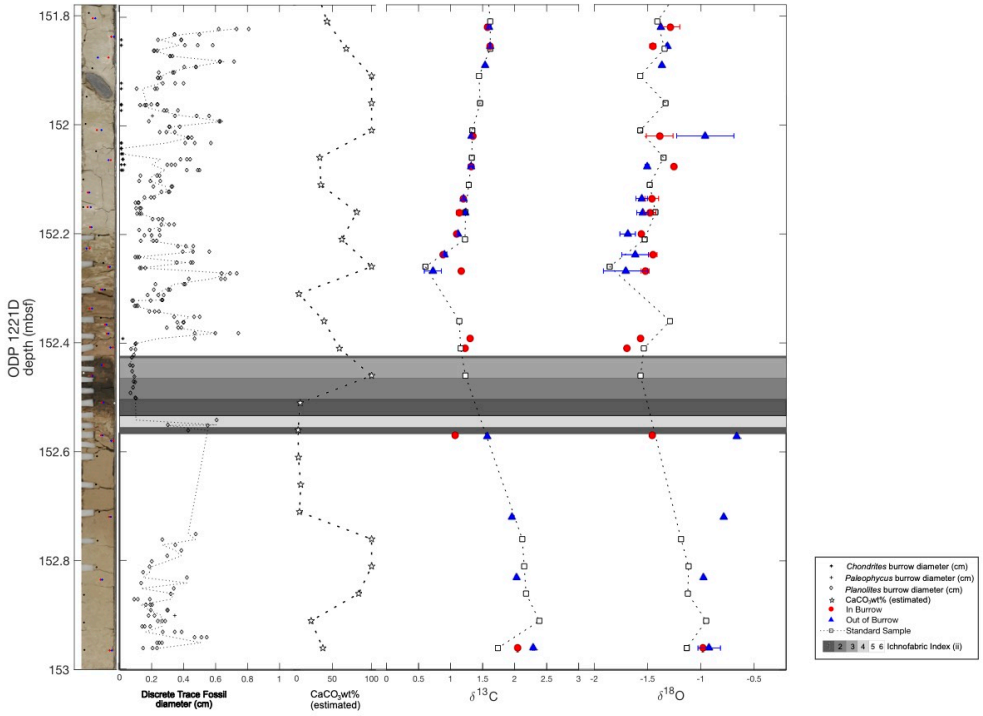

Figure 2.4: Image of core 1221D (taken at repository) with sites of sample indicated (red circle for in burrow, blue circle for out of burrow, and black or white square for standard sample). The ichnofabric index is represented as a color gradient behind the panel, with darkest grey representative as 1 or no mixing, and white representing 5,6, and all the subcategories of 6, as they are descriptive terms for completely mixed. The ichnofabric index is plotted against depth (mbsf). All measured discrete trace fossil diameters in black diamonds (*Planolities*), black crosses (*Paleophycus*), and black ∗ (*Chondrites*), with the black dotted line representing average burrow diameter all plotted vs. meters below the seafloor (mbsf). Estimated $CaCO_3$ wt. % plotted in black stars with black dotted line vs. mbsf. Bulk carbonate $\delta^{13}C$ and $\delta^{18}O$ from inside burrows (red circles), outside burrows (blue triangles), standard samples (black squares with grey line) and bulk carbonate $\delta^{13}C$ and $\delta^{18}O$ from Nunes and Norris 2005 (black x) plotted vs. mbsf.

Pre-PETM

The PETM onset in Hole 1221D occurs at 152.770 mbsf based on the last occurrence of *Gavelinella beccariiformis* and a lithologic shift from chalk to zeolithic clay (Lyle et al. 2001). Across the late Paleocene sediment analyzed here (153.000-152.770 mbsf), the $\delta^{13}C$ of the 'standard' bulk samples averages 2.114‰ and $\delta^{18}O$ of the bulk samples averages -1.101 ‰. The estimated wt% $CaCO_3$ averages 68.711%. Sediment is completely homogenized (ii of 5+) throughout the interval, with average *Planolites* diameters average 0.286 cm (min:0.091, max: 1.91). In the pre-PETM depth interval, two in-and-out-of-burrow pairs were sampled, with one pair having insufficient carbonate in the in-burrow sample for analysis. At 152.96 mbsf the in-burrow $\delta^{13}C$ sample is depleted by 0.246‰, while the $\delta^{18}O$ values are within error of each other.

PETM onset and missing peak of excursion

The benthic foraminiferal extinction indicates the PETM onset occurs at 152.770 mbsf, but in our isotopic records, there is no clear excursion at this depth. Based on previously published benthic foraminifera isotopic records from Site 1221C (Nunes and Norris 2005, 2006), the onset and peak (minimum) of the CIE occurs between 152.770 and 152.215 mbsf. 'Standard' bulk sample $\delta^{13}C$ and $\delta^{18}O$ at 152.760 mbsf are consistent with pre-excursion values, while in the interval between 152.710 to 152.510 mbsf, the 'standard' bulk samples contained insufficient carbonate for isotopic analysis. From 152.630 to 152.460 mbsf, the 'standard' bulk sample $\delta^{13}C$ and $\delta^{18}O$ decrease from pre-PETM values, reaching the record minimum at 152.260 mbsf. Lithology shifts from clay at 152.770 mbsf to carbonate at 152.300 mbsf. Throughout this interval, bioturbation

completely homogenizes the sediment (ii 5+) except for 152.570 to 152.430 mbsf, where bioturbation ceases twice (ii of 1 from 152.570-152.56 and 152.432-152.43 mbsf), while bioturbation intensity oscillates from ii 2 to 4 between these two cessations. Between 152.710 to 152.510 mbsf, the average *Planolites* diameter averages 0.289 cm (max: 0.743, min:0.065). In the two in-and-out-of-burrow sample pairs with sufficient carbonate for analysis, the pair at 152.720 mbsf has the largest offsets of the record: 0.480 in $\delta^{13}C$ and 0.798 in $\delta^{18}O$, while the pair at 152.268 mbsf has an offset of 0.480 in $\delta^{13}C$ but indistinguishable $\delta^{18}O$.

Recovery

Following the minimum of both the 'standard' bulk samples corresponding to the previously published benthic foraminifera isotopic records from Site 1221C (Nunes and Norris 2005, 2006), $\delta^{13}C$ values increase from the minimum over 152.215 to 151.810 mbsf. Across this interval, the $\delta^{13}C$ of the 'standard' bulk samples increases from 1.225‰ at 152.210 to 1.619‰ by 151.860 mbsf with estimated wt% $CaCO_3$ averaging 69.13%. The sediment consists of brown calcareous chalk, and is thoroughly bioturbated (ii of 5+), with average burrow diamters of 0.278 (max: 1.155, min:0.010). In-and-out-of-burrow pairs yield similar $\delta^{13}C$ and $\delta^{18}O$ values, with an exception at 199.31 mbsf, where the $\delta^{13}C$ of the out-of-burrow sample is 0.477‰ lower and the $\delta^{18}O$ is 0.214‰ higher compared to the in-burrow sample.

Discussion

Significance of sediment movement in geochemical records

At the three investigated sites, all successfully produced paired in and out of burrow records are from completely mixed sediments (ii 5+). In all three cores, the largest differences between the in and out of burrow samples occur in intervals close to the onset and peak of the PETM. At ODP Site 1209, the largest difference in $\delta^{13}C$ (0.853‰) is stratigraphically just below the onset of the PETM, while the largest difference in $\delta^{18}O$ (0.329‰) and second largest difference in $\delta^{13}C$ (0.634‰) occurs 9.990cm above the PETM onset and within the CIE peak. Whereas, across the recovery interval, offsets between in and out of burrow $\delta^{13}C$ average 0.084‰ while offsets between in and out of burrow $\delta^{18}O$ average 0.051‰, which is statically insignificant determined by duplicates for these records. Though the records at Sites 1220B and 1221D are complicated by the significant number of unpaired in and out of burrow measurements due to low carbonate content throughout the PETM onset and expected CIE peak, the largest difference in $\delta^{13}C$ between in and out of burrow pairs occurs within the expected CIE peak (1220B: 0.447‰, 1221D: 0.480‰). Whereas in the defined recovery intervals, the offsets between in and out of burrow pairs are much smaller (1220B: $\delta^{13}C$ 0.049 ‰, $\delta^{18}O$ 0.111‰; 1221D: $\delta^{13}C$ 0.018 ‰, $\delta^{18}O$ 0.105‰;). As bioturbation intensity at the depths corresponding to all of the in and out of burrow pairs indicate complete homogenization, isotopic differences between in and out of burrow pairs is due to proximity to large changes in sedimentary isotopic values over short stratigraphic intervals. At Site 1209C, across the interval including the PETM onset and

peak, $\delta^{13}C$ records indicated an average offset of 0.308‰ between in and out of burrow pairs, skewing the record towards a more rapid recovery than indicated in the out of burrow record. Whereas, in the recovery periods, when sedimentary isotopic values change gradually, though the sediment shows similar degree of mixing, the geochemical impact of sampling in burrows is reduced. Therefore, while sampling records during which rapid geochemical changes are suspected, special care should be taken to avoid sampling of burrows.

Lithological relationship to sediment movement

We find no correlation (R^2 0.0493, p-value 0.075) between ichnofabric index and sediment calcium carbonate content. Though, given extended lithological shifts at ODP Sites 1220B and 1221D, it appears that sediment from within burrows derives from stratigraphically shallower locations in the core. At ODP Site 1220, in the interval from 199.61 to 199.395 mbsf where only in-burrow records produce a value, $\delta^{13}C$ greatly diverges from that of the 'standard' samples. Throughout this interval, the sediment sampled from burrows is a lighter brown compared to the surrounding dark brown matrix. The values from the in-burrow sample at 199.395 mbsf ($\delta^{13}C$ of 0.398 ‰, $\delta^{18}O$ of -0.140 ‰, 69.14% estimated $CaCO_3$) are most similar to the standard sample at 199.300 mbsf ($\delta^{13}C$ of 0.452‰, $\delta^{18}O$ of -0.179‰, 34.06% estimated $CaCO_3$), the color of sediments matches. Based on these commonalities, it appears that sediment was piped down up by up to ~ 0.095 m. Though, the estimated wt% of $CaCO_3$ is significantly more concentrated from the in-burrow sample than all standard sediments following the onset of the PETM.

Impact of sampling practices

Sampling directly within discrete trace fossils can impact the stratigraphic fidelity of geochemical records. The most prominent differences in this study were revealed when isotopic records changed rapidly over a short stratigraphic depth or when there were significant differences in carbonate content between the matrix and in-burrow sediment. Indications of reduced or ceased bioturbation can be used as a clue for rapid changes in the benthic environment (Ekdale et al., 1984; Bromley, 1996, Lobza and Schieber, 1999). However, isotopic differences between discrete trace fossils and the outer matrix even in thoroughly bioturbated sediments caution the avoidance of sampling discrete trace fossils, particularly across intervals of potentially rapid environmental change.

In the record from Site 1209, the most notable offsets, that could also impact the apparent shape of the CIE, occur from 197.290 to 197.100 mbsf. The isotopic offsets at these depths are consistent with piping down of younger sediment, which could artificially shorten the apparent PETM recovery interval. Visually identifying discrete trace fossils can be extremely challenging in carbonates, as burrow identification often relies on color differences, which are dependent on a variety of factors such as the occurrence of lithological changes, the preservation of "halos" of materials containing organic matter, or evidence of oxygen transported at depth. Many discrete trace fossils cannot be identified by sight and require specialized processes such as x-ray photography of the core (Ekdale & Bromley 1991), which would be impractical for guiding routine

sediment sampling. However, improved methods for identifying burrows could aid sampling across intervals of rapid environmental change.

Conclusions

Patterns of bioturbation intensity varied greatly across the PETM at the three ODP sites sampled for this study. Burrow-specific sampling for stable isotope analysis identified the piping down and relocation of sediment by bioturbating organisms at all bioturbation intensities (ii of 2+). We find that the greatest impact of sampling burrows on bulk carbonate stable isotope ($\delta^{13}C$ and $\delta^{18}O$) records occurs across the intervals recording the most rapid environmental change, in this case, near the onset and peak of the PETM. We suggest avoiding sampling of discrete trace fossils, regardless of the surrounding degree of bioturbation, across sediment intervals recording rapid climatic change in order to prevent inadvertent sampling of younger sediment and potential truncation of these episodes.

References

Aller, R. C. (1982). The effects of macrobenthos on chemical properties of marine sediment and overlying water. In *Animal-sediment relations* (pp. 53-102). Springer, Boston, MA.

Bottjer, D. J., & Droser, M. L. (1991). Ichnofabric and basin analysis. *Palaios*, 199-205.

Bottjer, D. J., & Droser, M. L. (1991). Ichnofabric and basin analysis. *Palaios*, 199-205.

Bralower, T. J., Fullagar, P. D., Paull, C. K., Dwyer, G. S., & Leckie, R. M. (1997). Mid-Cretaceous strontium-isotope stratigraphy of deep-sea sections. *Geological Society of America Bulletin*, *109*(11), 1421-1442.

Bralower, T. J., Kelly, D. C., Gibbs, S., Farley, K., Eccles, L., Lindemann, T. L., & Smith, G. J. (2014). Impact of dissolution on the sedimentary record of the Paleocene–Eocene thermal maximum. *Earth and Planetary Science Letters*, *401*, 70-82.

Chang, L., Harrison, R. J., Zeng, F., Berndt, T. A., Roberts, A. P., Heslop, D., & Zhao, X. (2018). Coupled microbial bloom and oxygenation decline recorded by magnetofossils during the Palaeocene–Eocene Thermal Maximum. *Nature Communications*, *9*(1), 1-9.

Crimes, T. P. (1987). Trace fossils and correlation of late Precambrian and early Cambrian strata. *Geological Magazine*, *124*(2), 97-119.

Crimes, T. P., & Droser, M. L. (1992). Trace fossils and bioturbation: the other fossil record. *Annual Review of Ecology and Systematics*, *23*(1), 339-360.

Darwin C. The Formation of Vegetable Mould, Through the Action of Worms, with Observations on their Habits J. Murray, London, 1881, 184 pp.

Dickson, A. J., & Cohen, A. S. (2012). A molybdenum isotope record of Eocene Thermal Maximum 2: Implications for global ocean redox during the early Eocene. *Paleoceanography*, *27*(3).

Díez-Canseco, D., Buatois, L. A., Mángano, M. G., Díaz-Molina, M., & Benito, M. I. (2016). Ichnofauna from coastal meandering channel systems (Upper Cretaceous Tremp Formation, South-Central Pyrenees, Spain): delineating the fluvial-tidal transition. *Journal of Paleontology*, *90*(2), 250-268.

Dolman, A. M., Groeneveld, J., Mollenhauer, G., Ho, S. L., & Laepple, T. (2021). Estimating Bioturbation From Replicated Small-Sample Radiocarbon Ages. *Paleoceanography and Paleoclimatology*, *36*(7), e2020PA004142.

Droser, M. L., & Bottjer, D. J. (1989). Ordovician increase in extent and depth of bioturbation: Implications for understanding early Paleozoic ecospace utilization. *Geology*, *17*(9), 850-852.

Ekdale, A. A. (1977). Quantitative Paleoecological Aspects of Modern Marine Mollusk Distribution, Northeast Yucatan Coast, Mexico: Reef Biota.

Ekdale, A. A. (1980). 11. TRACE FOSSILS IN DEEP SEA DRILLING PROJECT LEG 58 CORES.

Ekdale, A. A., Muller, L. N., & Novak, M. T. (1984). Quantitative ichnology of modern pelagic deposits in the abyssal Atlantic. *Palaeogeography, Palaeoclimatology, Palaeoecology*, *45*(2), 189-223.

Farley, K. A., & Eltgroth, S. F. (2003). An alternative age model for the Paleocene–Eocene thermal maximum using extraterrestrial 3He. *Earth and Planetary Science Letters*, *208*(3-4), 135-148.

Hall, J. (1847). *Paleontology* (Vol. 1). Van Benthuysen.

Hull, P. M., Franks, P. J., & Norris, R. D. (2011). Mechanisms and models of iridium anomaly shape across the Cretaceous–Paleogene boundary. *Earth and Planetary Science Letters*, *301*(1-2), 98-106.

Hülse, D., Arndt, S., Daines, S., Regnier, P., & Ridgwell, A. (2018). OMEN-SED 1.0: a novel, numerically efficient organic matter sediment diagenesis module for coupling to Earth system models. *Geoscientific Model Development*, *11*(7), 2649-2689.

Jones, T. D., Lunt, D. J., Schmidt, D. N., Ridgwell, A., Sluijs, A., Valdes, P. J., & Maslin, M. (2013). Climate model and proxy data constraints on ocean warming across the Paleocene–Eocene Thermal Maximum. *Earth-Science Reviews*, *125*, 123-145.

Kanzaki, Y., Hülse, D., Kirtland Turner, S., & Ridgwell, A. (2021). A model for marine sedimentary carbonate diagenesis and paleoclimate proxy signal tracking: IMP v1. 0. *Geoscientific Model Development*, *14*(10), 5999-6023.

Kelly, D. C. (2002). Response of Antarctic (ODP Site 690) planktonic foraminifera to the Paleocene–Eocene thermal maximum: Faunal evidence for ocean/climate change. *Paleoceanography*, *17*(4), 23-1.

Kennett, J. P., & Stott, L. D. (1991). Abrupt deep-sea warming, palaeoceanographic changes and benthic extinctions at the end of the Palaeocene. *Nature*, *353*(6341), 225-229.

Kirtland Turner, S., Hull, P. M., Kump, L. R., & Ridgwell, A. (2017). A probabilistic assessment of the rapidity of PETM onset. *Nature communications*, *8*(1), 1-10.

Küssner, K., Sarnthein, M., Lamy, F., & Tiedemann, R. (2018). High-resolution radiocarbon records trace episodes of Zoophycos burrowing. *Marine Geology*, *403*, 48-56.

Lachetl, C., & Bard, P. Y. (1994). Numerical and theoretical investigations on the possibilities and limitations of Nakamura's technique. *Journal of Physics of the Earth*, *42*(5), 377-397.

Lachetl, C., & Bard, P. Y. (1994). Numerical and theoretical investigations on the possibilities and limitations of Nakamura's technique. *Journal of Physics of the Earth*, *42*(5), 377-397.

Lobza, V., & Schieber, J. (1999). Biogenic sedimentary structures produced by worms in soupy, soft muds; observations from the Chattanooga Shale (Upper Devonian) and experiments. *Journal of Sedimentary Research*, *69*(5), 1041-1049.

Lougheed, B. C., Metcalfe, B., Ninnemann, U. S., & Wacker, L. (2018). Moving beyond the age–depth model paradigm in deep-sea palaeoclimate archives: dual radiocarbon and stable isotope analysis on single foraminifera. *Climate of the Past*, *14*(4), 515-526.

Löwemark, L., & Grootes, P. M. (2004). Large age differences between planktic foraminifers caused by abundance variations and Zoophycos bioturbation. *Paleoceanography*, *19*(2).

Löwemark, L., & Werner, F. (2001). Dating errors in high-resolution stratigraphy: a detailed X-ray radiograph and AMS-14C study of Zoophycos burrows. *Marine Geology*, *177*(3-4), 191-198.

McInerney, F. A., & Wing, S. L. (2011). The Paleocene-Eocene Thermal Maximum: A perturbation of carbon cycle, climate, and biosphere with implications for the future. *Annual Review of Earth and Planetary Sciences*, *39*, 489-516.

Meissner, K. J., Bralower, T. J., Alexander, K., Jones, T. D., Sijp, W., & Ward, M. (2014). The Paleocene-Eocene thermal maximum: How much carbon is enough?. *Paleoceanography*, *29*(10), 946-963.

Meysman, Filip JR, Jack J. Middelburg, and Carlo HR Heip. "Bioturbation: a fresh look at Darwin's last idea." *Trends in Ecology & Evolution* 21.12 (2006): 688-695.

Nicholson, H. A. (1873). III. Contributions to the study of the errant Annelides of the older palæozoic rocks. *Proceedings of the Royal Society of London*, *21*(139-147), 288-290.

Pälike, C., Delaney, M. L., & Zachos, J. C. (2014). Deep-sea redox across the Paleocene-Eocene thermal maximum. *Geochemistry, Geophysics, Geosystems*, *15*(4), 1038-1053.

Pemberton, S. G., & Frey, R. W. (1982). Trace fossil nomenclature and the Planolites-Palaeophycus dilemma. *Journal of Paleontology*, 843-881.

Pickerill, R., Fillion, D., & Brenchley, P. (1991). A note on the occurrence of Arthrophycus in the Bell Island Group of eastern Newfoundland. *Atlantic Geology*, *27*(1), 73-77.

Ridgwell, A. (2007). Interpreting transient carbonate compensation depth changes by marine sediment core modeling. *Paleoceanography*, *22*(4).

Röhl, U., Westerhold, T., Bralower, T. J., & Zachos, J. C. (2007). On the duration of the Paleocene-Eocene thermal maximum (PETM). *Geochemistry, Geophysics, Geosystems*, *8*(12).

Schieber, J. (2003). Simple gifts and buried treasures–implications of finding bioturbation and erosion surfaces in black shales. *The Sedimentary Record*, *1*(2), 4-8.

Schink, D. R., Guinasso Jr, N. L., & Fanning, K. A. (1975). Processes affecting the concentration of silica at the sediment-water interface of the Atlantic Ocean. *Journal of Geophysical Research*, *80*(21), 3013-3031.

Steiner, Z., Lazar, B., Levi, S., Tsroya, S., Pelled, O., Bookman, R., & Erez, J. (2016). The effect of bioturbation in pelagic sediments: lessons from radioactive tracers and planktonic foraminifera in the Gulf of Aqaba, Red Sea. *Geochimica et Cosmochimica Acta*, *194*, 139-152.

Tarhan, L. G. (2018). The early Paleozoic development of bioturbation—evolutionary and geobiological consequences. *Earth-Science Reviews*, *178*, 177-207.

Teal, L. R., Bulling, M. T., Parker, E. R., & Solan, M. (2008). Global patterns of bioturbation intensity and mixed depth of marine soft sediments. *Aquatic Biology*, *2*(3), 207-218.

Teal, L. R., Parker, E. R., & Solan, M. (2010). Sediment mixed layer as a proxy for benthic ecosystem process and function. *Marine Ecology Progress Series*, *414*, 27-40.

Thomas, D. (1990). Intra-household resource allocation: An inferential approach. *Journal of human resources*, 635-664.

Thomas, D. J., Bralower, T. J., & Jones, C. E. (2003). Neodymium isotopic reconstruction of late Paleocene–early Eocene thermohaline circulation. *Earth and Planetary Science Letters*, *209*(3-4), 309-322.

Thomas, E., & Aubry, M. P. (1998). Biogeography of the late Paleocene benthic foraminiferal extinction. *Late Paleocene-Early Eocene climatic and biotic events in the marine and terrestrial records*, *416*, 214-235.

Thomas, E., & Monechi, S. (2007). Cenozoic mass extinctions in the deep sea: What perturbs the largest habitat on Earth?. *SPECIAL PAPERS-GEOLOGICAL SOCIETY OF AMERICA*, *424*, 1.

Trauth, M. H. (1998). TURBO: A dynamic-probabilistic simulation to study the effects of bioturbation on paleoceanographic time series. *Computers & Geosciences*, *24*(5), 433-441.

Trauth, M. H. (2013). TURBO2: A MATLAB simulation to study the effects of bioturbation on paleoceanographic time series. *Computers & Geosciences*, *61*, 1-10.
Von Sternberg, K. M. G. (1833). Versuch einer geognostisch-botanischen Darstellung der. *Flora des Vorwelt*, *5*, 6-80.

Westerhold, T., Marwan, N., Drury, A. J., Liebrand, D., Agnini, C., Anagnostou, E., ... &

Zachos, J. C. (2020). An astronomically dated record of Earth's climate and its predictability
over the last 66 million years. *Science*, *369*(6509), 1383-1387.

Zachos, J. C., Röhl, U., Schellenberg, S. A., Sluijs, A., Hodell, D. A., Kelly, D. C., ... & Kroon, D. (2005). Rapid acidification of the ocean during the Paleocene-Eocene thermal maximum. *Science*, *308*(5728), 1611-1615.

Zeebe, R. E., & Lourens, L. J. (2019). Solar System chaos and the Paleocene–Eocene boundary age constrained by geology and astronomy. *Science*, *365*(6456), 926-929.

CHAPTER 3: Chapter 3: Reconstructing North Atlantic Ocean circulation during the Paleocene-Eocene Thermal Maximum

Abstract

The Paleocene-Eocene Thermal Maximum (PETM, ~56 Ma) was an abrupt period of greenhouse warming during which thousands of gigatons of isotopically depleted carbon were added to the atmosphere over a few thousand years, leading to a global negative carbon isotope excursion (CIE). The oceans absorbed much of this carbon, making it more acidic, leading to a shoaling of the calcite compensation depth (CCD) and massive carbonate dissolution throughout the deep sea. Following this initial acidification, it has been hypothesized that enhanced carbonate and silicate weathering due to higher global temperatures resulted in a temporary "overshoot" in the depth of the CCD. The record of the PETM from North Atlantic IODP Site U1403 shows evidence of this carbonate overshoot; this site was below the CCD during the latest Paleocene to early Eocene but began preserving carbonate ~70 kyr following the PETM onset. However, changes in the pattern of global overturning ocean circulation have also been proposed during the PETM, with implications for the deep ocean saturation state, and which could also change spatial patterns in carbonate preservation in the deep sea. Changes in benthic carbon isotope gradients across the PETM suggest a temporary formation of North Atlantic Deep Water that persisted for a few thousand years followed by a return to Southern Ocean dominated circulation. If deep waters formed in the North Atlantic, this should be associated with an increase in the deep ocean saturation state and enhanced

carbonate preservation. To investigate the movement of the CCD in the North Atlantic and determine the relative roles of globally enhanced weathering and local changes in ocean circulation, we generate a new neodymium isotope record from fossilized fish teeth. Neodymium isotopes are conservative tracers of water masses that are sensitive to changes in the origin of deep waters bathing a site. Our results are consistent with previously published neodymium isotopes records of the North Atlantic, which suggest a single source of deep water formation in the Southern Hemisphere driving overturning circulation in the Atlantic. We find no evidence for a short-lived formation of North Atlantic deep water following the onset of the PETM.

Introduction

Ocean circulation, through the production and movement of deepwater masses are important components of heat transport in Earth's climate system. The shape and size of ocean basins combined with Earth's climate system greatly influence where deepwater masses form and how they circulate. In the Paleogene, rapid changes in climate in conjunction with ocean basin configuration changes point towards the importance of understanding the location of deepwater mass formation and intensity of overturning circulation (Via and Thomas, 2007). Temporary changes in North Atlantic circulation following the onset Paleocene-Eocene Thermal Maximum (PETM) have been suggested (Tripati and Elderfeild 2005; Nunes and Norris 2006).

The Paleocene-Eocene Thermal Maximum (PETM, ~55.9 Ma, Westerhold 2017) is the most pronounced global warming event in the Paleogene, and is characterized by a

negative carbon isotope excursion (CIE) <–2‰ and a temperature increase of more than 5 °C globally in less than 10 kyr (McInerney and Wing, 2011; Zachos et al., 2008). The complete duration of the PETM is ~200–300 kyr, which generally contains the CIE onset ((<~20 kry), CIE peak (~60–120 kyr), and following recovery (~80–120 kyr) (McInerney and Wing, 2011). Marine ecosystems were greatly impacted during the PETM onset, with a major benthic foraminiferal extinction (Thomas, 2003, 2007; Alegret et al., 2021), and migration and body-size decrease of planktonic foraminifera (Thomas and Shackleton, 1996; Petrizzo, 2007), all possibly impacted by a variety of factors including increased temperature, low-oxygen conditions, corrosive seawater, reduced productivity (Thomas, 2007).

Paleocene-Eocene ocean basin configuration

In the Paleocene, Atlantic Ocean basin became deeper and wider, allowing for latitudinal water mass movements dominated by Southern Ocean sources (Batenburg 2018). Though, the northern part of the North Atlantic basins (the Norwegian-Greenland and Labrador seas) had just begun to form (Talwani and Eldholm, 1977; Saunders et al., 1997), the Caribbean gateway and Tethys Ocean, were open, allowing for exchange between the Atlantic and Pacific at lower latitudes, and the Drake Passage and the Tasman Sea were not open to deep flow (Barker and Burrell, 1977; Lawver and Gahagan, 1998, 2003).

Hypothesized circulation at the PETM

Based on basin gradients of available benthic $\delta^{13}C$ data (Nunes and Norris, 2006; Tripati and Elderfield, 2005), patterns of widespread carbonate dissolution (Dickens,

2000; Kump et al., 2009; Ridgwell and Schmidt, 2010; Zachos et al., 2005, 2008), deep-sea carbonate ion gradients (Zeebe and Zachos, 2007), and some numerical modeling studies (Bice and Marotzke, 2002; Lunt et al., 2012; Alexander et al., 2015), it has been argued that a temporary change in thermohaline circulation may have been associated with the PETM.

Such studies have hypothesized circulation patterns different than the modern ocean operating before and after the PETM (Kennett and Stott, 1991; Lunt et al., 2011). In the Atlantic, throughout the Paleocene, proxy data from neodymium isotopes and benthic foraminifera suggest the Southern Ocean as the dominant location for deepwater formation during the early Paleogene (Miller and Tucholke, 1983; Mountain and Miller, 1992; Pak and Miller, 1992; Zachos et al., 1992; Thomas et al., 2003; Via and Thomas, 2006, Abbott 2016). Though, some high-resolution carbon isotope records suggest the convection of deep waters in the Northern Hemisphere, displacing the southern-sourced water during the PETM onset (Bice and Marotzke, 2002; Tripati and Elderfield, 2005; Nunes and Norris, 2006; Alexander et al., 2015). However, interpreting past benthic foraminiferal $\delta^{13}C$ records across the PETM as an indicator of thermohaline circulation is complicated by many factors, including potential additions of fractionated carbon sources (Kurtz et al., 2003), changes in productivity (Paytan et al., 2007), biological extinction and migration events, and dissolution in highly corrosive bottom waters erasing parts of the record (Pagani et al., 2006; Zeebe and Zachos, 2007; McCarren et al., 2008; Alexander et al., 2015). Due to the majority of deep sea sediments being impacted through varying amounts of dissolution (Wade et al., 2020), $\delta^{13}C$ records could be

missing important parts of the CIE body, making an gradients between end-members due to miss-aligned records.

Neodymium isotopes

Neodymium (Nd) isotope analysis of fish teeth and debris is a commonly used method for tracing deep water masses that is generally not affected by biogeochemical processes (Frank, 2002; Goldstein et al., 2003; Thomas, 2004). These materials attain their Nd isotope signals during early diagenesis on the seafloor, causing the signal produced is generally interpreted as the bottom water Nd isotope ratio in the region of deposition (Martin & Haley, 2000; Martin & Scher, 2004). Neodymium is a lithogenic element, supplied to the ocean largely from the continents, which carries characteristic isotopic signatures representative of the age and lithology of the local rock (Robinson et al., 2021).

Neodymium isotopes are non-conservative tracers of water masses, with a short residence time in the ocean (~400–700 years; Tachikawa et al., 2003), allowing water masses to retain their unique isotopic ratio in the absence of additional Nd inputs (Baskaran 2011). In Precambrian crustal rocks the Nd is very unradiogenic (low $^{143}Nd/^{144}Nd$) while recent mantle-derived rocks are highly radiogenic (high$^{143}Nd/^{144}Nd$). Currently, North Atlantic deep waters are characterized by unradiogenic εNd values of −13, whereas the Southern Ocean deep waters are characterized by εNd values of around −8, and Pacific waters show radiogenic εNd values of −4 (van de Flierdt et al. 2016). Away from ocean margins, the Nd isotopic signatures can indicate the origin of water

masses, ocean circulation, and water mass mixing (e.g., Frank, 2002; Goldstein & Hemming, 2014; van de Flierdt et al., 2016).

Site U1403

The addition of CO_2 into the oceans due to the onset of the PETM resulted in global rapid shoaling of CCD with decreases in pH and the carbonate saturation state (Hönisch et al 2012). After the PETM onset, the CCD gradual recovered as seafloor carbonate dissolution restored ocean carbonate saturation (Zachos et al 2005, Zeebe and Zachos 2007). Predictions based on numerical and conceptual models of the carbon cycle include that during the recovery period, there could have been a period of carbonate oversaturation, where the build-up of alkalinity in the ocean could have caused an 'overshoot' of the CCD (Dickens et al 1997, Zeebe and Zachos 2013).

Site U1403 in the North Atlantic has a change in CCD preserved that indicates preservation of this 'overshoot'. In the late Paleocene and into the PETM, the site was below the CCD and did not preserve any carbonate. At 70,000 years after the onset of the PETM that Site U1403 began preserving carbonate and continued preserving carbonate well into the Eocene (Penman et al. 2016). This "overshoot" of the CCD is tied to the PETM recovery phase. This change in carbonate preservation could point to a global change in ocean chemistry with globally enhanced calcite burial preserved in the sediments. Or this could be due to a localized effect due to temporary formation of North Atlantic Deep Water, creating a declining carbonate saturation state from North to South. In this study, we investigate this question by producing a new high resolution εNd record based on ichthyoliths at Site U1403. We then compare this record to published

neodymium isotopes records, benthic $\delta^{13}C$ records to determine the location of Atlantic deepwater mass formation.

Materials

Expedition 342 of the Integrated Ocean Drilling Program (IODP) targeted Paleogene- aged sedimentary sequences from a range of paleodepths with high deposition and microfossil accumulation rates (Norris et al., 2012). Site U1403 is located on the Southeast Newfoundland Ridge off the coast of Newfoundland, Canada (39°56.60′N, 51°48.20′W). The core was recovered from a present sea floor water depth of 4949 m (Norris et al., 2014), and the paleodepth of the site is ~4,374 mbsf (Tucholke and Vogt, 1979), placing it deeper than the initial Paleogene carbonate compensation depth. Proxy records produced at this core include bulk $\delta^{13}C_{org}$, bulk $\delta^{13}C_{carb}$, and wt% $CaCO_3$ assitied in identifying the location of the PETM within the record (Penman 2016). At the PETM, sediment is clay dominated, while ~70 kyr after the onset, carbonate sedimentation begins and persists for ~150 kyr throughout the recovery (Penman 2016).

Methods

We processed 73 samples from IODP Site U1403 spanning the late Paleocene and into the early Eocene, creating a high resolution record from pre-carbon input through the recovery. These sediments were dried, washed over a 63μm mesh sieve, and dried again in an oven. Under the microscope, ichthyoliths were picked out of the sample residue with a small paintbrush. While others have suggested that the >125 μm size fraction

should yield the 5-15 fish teeth necessary for Nd analyses (Martin and Haley, 2000; Scher and Martin, 2004, 2006, 2008), at Site U1403, teeth abundance was low making it necessary to pick samples down to the 63 μm to obtain between ~20 teeth for the requisite for neodymium isotope analysis.

The samples were processed at the University of South Carolina to prepare the teeth for Nd analysis. The ichthyoliths were cleaned, dissolved in 50μl of 0.25 M HCl for two hours, and then loaded into the columns. To extract the neodymium from the ichthyoliths, lanthanide-specific cation exchange resin (LN Resin, Eichrom Industries) was used in small single-stage columns. The cleaned resin was loaded into columns with the resin beds just below the stem tops, washed again with 6 M HCl, and reconditioned with 0.25 M HCl. Using the column elution curves (Scher and Martin 2010), the 50μg from the ichthyoliths previously dissolved in 50μl 0.25 M HCl and the solution were loaded onto the resin bed. The column was then washed with 3ml of 0.25 M HCl in a few steps. First, 50μl 0.25 M HCl was added to the column to elute Ca, Ba, and other major cations to waste. Next, columns were washed with 300μl of 0.25 M HCl to elute the light rare Earth elements to waste. Nd was eluted with 400μl of 0.25 M HCl, with solutions collected in 1ml screw top microcentrifuge tubes. Finally, samarium (Sm) was collected in 6M HCl for the correction of in-situ production of 143Nd from decay of 147Sm. The last step before isotopic analysis was to add 400μl of 2% HNO_3 to the tube.

These samples were then analyzed via multi-collector inductively-coupled mass spectrometry (MC-ICMPS). Measurements were made in static multicollection, and all Nd isotopes were measured while monitoring masses 147 and 149 (Sm). The La Jolla Nd

standard was run at the beginning and end of each analytical day, and the AMES Nd solution (Tanaka et al. 2000). The results were decay-corrected for the time of deposition by $(^{143}Nd/^{144}Nd)sample(t) = (^{143}Nd/^{144}Nd)sample(0) - [(^{147}Sm/^{144}Nd)sample(0) * (e^{\lambda t} - 1)]$ where t is time, the decay constant λ is 6.54×10^{-12}, and using an average $^{147}Sm/^{144}Nd$ ratio of 0.124 (Voigt et al. 2014). Nd-isotope ratios are reported as $\varepsilon Nd(t)$ values with respect to the Chondritic Uniform Reservoir (CHUR), which are calculated as $\varepsilon Nd(t) = [(^{143}Nd/^{144}Nd)sample(t) / (^{143}Nd/^{144}Nd)CHUR(t) - 1] \times 10^4$ using a $(^{143}Nd/^{144}Nd)CHUR(0)$ value of 0.512638, and a $(^{147}Sm/^{144}Nd)CHUR(0)$ of 0.1966 (Jacobsen & Wasserburg 1980). External reproducibility (2σ) of the measurements was between 0.06 and 0.31 εNd units and procedural Nd blanks were ≤ 30 pg Nd and thus negligible.

Age models and record comparison

At Site U1403 we utilized the age model of Penman et al., 2016, but converted to the new calibration of the geomagnetic polarity timescale (Westerhold et al., 2020). For a global comparison, all published ε_{Nd} records (Thomas, 2003; Via & Thomas, 2006, Abbot et al. 2016, Batenburg et al, 2018) which utilized a variety of magneto- and biostratigraphy and when available astrochronology, were also updated to the newest calibration the geomagnetic polarity timescale.

Results

At site U1403 (Figure 3.1), in the late Paleocene, ε_{Nd} values average ~ -8.21, but begin trending towards less radiogenic (more negative) value, reaching a low of -8.60 at

56.18 Ma. From 55.61-55.93 there is a gap in the record due to low fish tooth abundances. During the CIE body (56.50-55.96), ~.031 Ma after the onset of the PETM, ε_{Nd} becomes less radiogenic at -9.06 before quickly increasing to slightly more radiogenic values of ~ -8.3 (55.91-55.90 Ma) then ε_{Nd} drops back down to -9.07 (55.90 Ma). During the CIE recovery section of the record (55.89-55.76 Ma), the record does not contain the short-term fluctuations found in CIE body. During the CIE recovery, the record continues to become less radiogenic, reaching its lowest value of -9.21 (55.92 Ma), after which the record slowly trends towards more radiogenic, reaching ε_{Nd} value of -8.96. After the CIE recovery in the Eocene (55.76-55.5 Ma), the trend towards more radiogenic values continue with an ε_{Nd} value of -8.21 (55.68 Ma), before slightly decreasing, ending with values of averaging -8.62 (55.63-55.53 Ma). The largest short-term fluctuations in this record occur throughout the section that is devoid of carbonate, and begin trending towards more radiogenic values immediately before the appearance of carbonate.

Discussion

Global thermohaline circulation patterns throughout the PETM

When comparing ε_{Nd} records derived from fish teeth of the Atlantic to those of the Pacific, Caribbean, and Indian Ocean, the different sources of water become evident (Figure 3.2). While the global records reveal variability, the distinct differences between the Pacific record averaging ~ -4.27 points to a significantly more radiogenic source of deep water mass whereas the Atlantic, Southern, and Indian oceans are relatively non-

radiogenic averaging ~ -8.71. The Caribbean Ocean is most distinct with incredibly radiogenic values of -2, indicative of nearby active volcanism at the time (Bralower 1997). The distinct differences between the Pacific and Atlantic basins suggest unique deep water mass source formation (Thomas 2003, Abbot 2016).

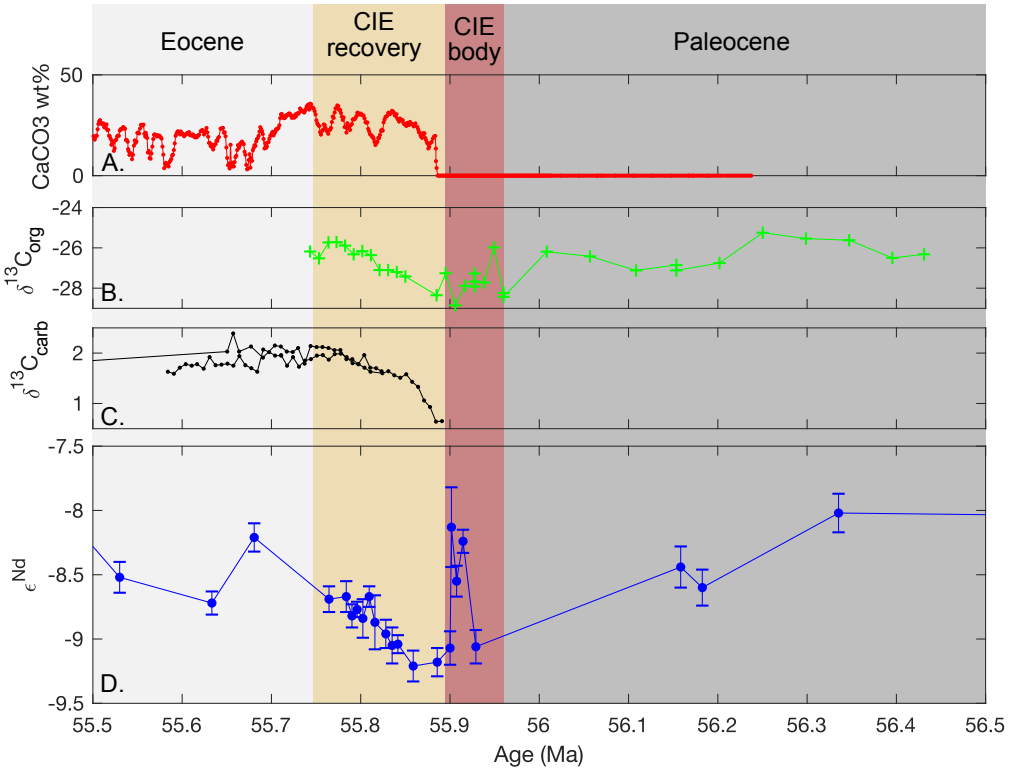

Figure 3.1 IODP Site U1403 with panel A. wt% $CaCO_3$ from Penman 2016. B. $\delta^{13}C_{org}$ from Penman 2016 C. $\delta^{13}C_{carb}$ from Penman 2016 D. ε_{Nd} record produced in their record. The age model from Penman 2016 was utilized to define the Paleocene (dark grey, 56.50-55.96 Ma), CIE body (red, 55.96-55.89 Ma), CIE recovery (tan, 55.89-55.76 Ma), and Eocene (light grey, 55.76-55.5)

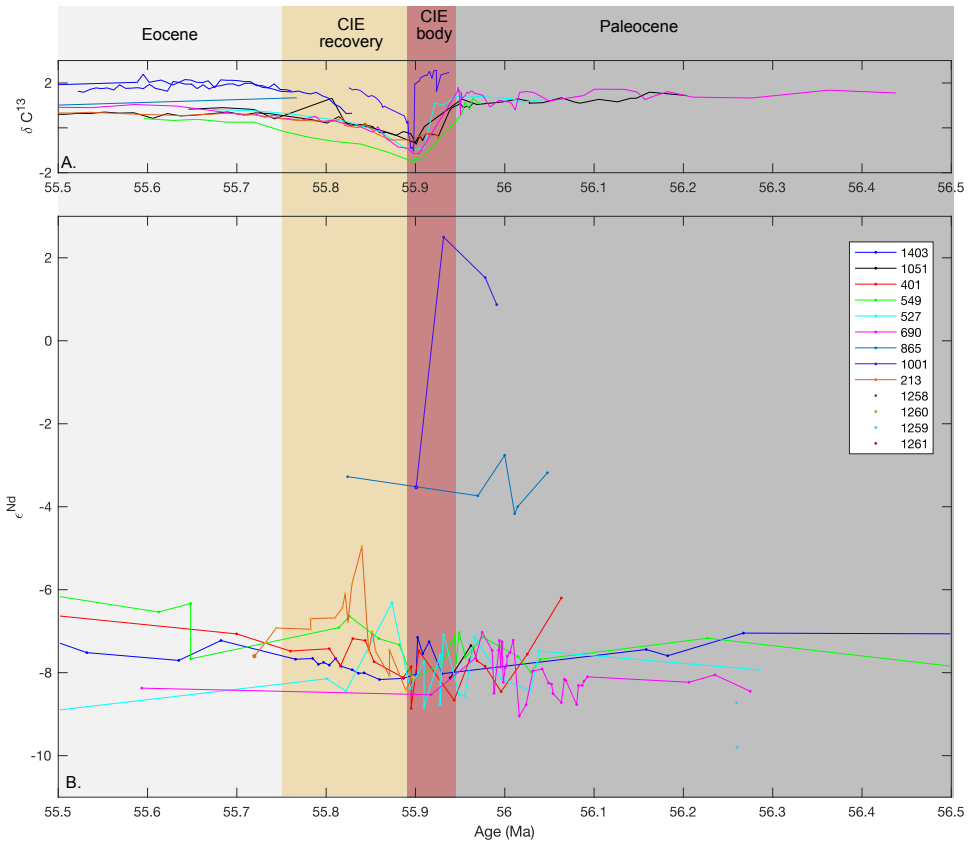

Figure 3.2: A compilation of all $\delta^{13}C$ and εNd records (Sites U1403, 1051, 401, 527, 549, 690, 1001, 1267, 525, 1258, 1259, 1260, and 1261). The top panel contains a compilation of published $\delta^{13}C$ for the sites. The bottom panel contains the new record of U1403 εNd derived from ichthyoliths, compared to published ichthyolith records.

North Atlantic circulation patterns

When comparing IODP site U1403 to DSDP sites 401 and 549, the most striking features are the short-term fluctuations between ~1-2 ε_{Nd} units throughout the studied interval (Figure 3.3, also present in global records as seen in Figure 3.2). A key feature of these fluctuations is that they are present throughout the Paleocene, CIE body, CIE recovery, and into the Eocene. Therefore, whatever paleoceanographic significance these

fluctuations may have over circulation changes, it would not be considered a mechanism for triggering deep and bottom warming (Thomas 2003). Suggestions for these oscillations in the North Atlantic include competing contributions from deep water (i.e. Southern Ocean and the Tethys, Thomas 2003), changes in Nd supply to the oceans (Scher and Martin, 2010), or weak North Atlantic deep water overturning cell, sensitive to local changes in Nd inputs (Abbott et al 2016).

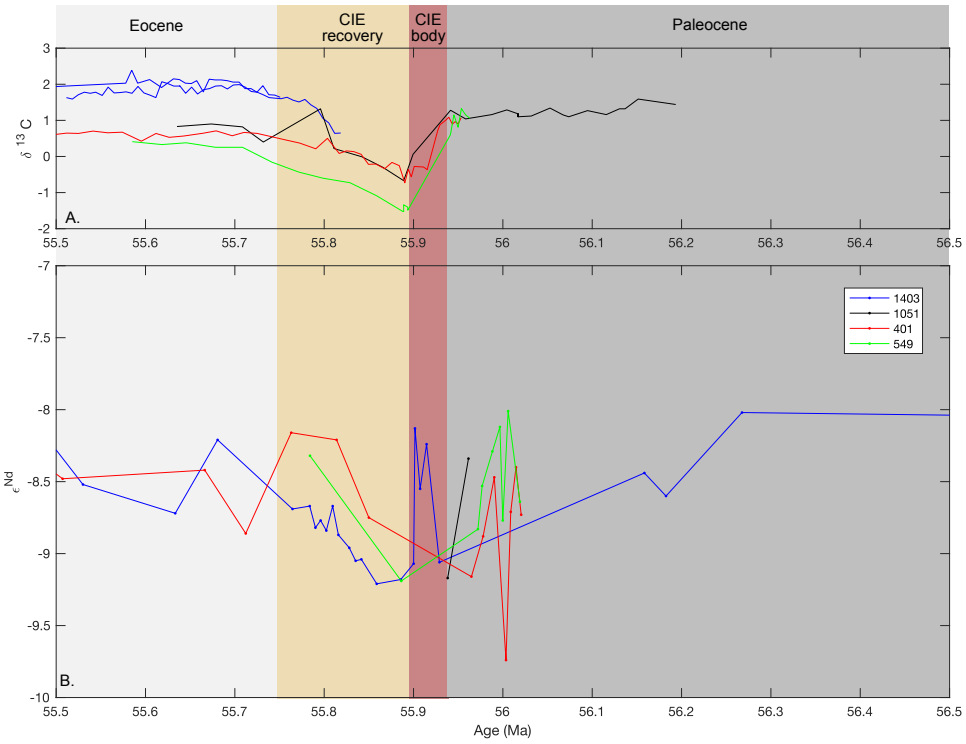

Figure 3.3 A compilation of North Atlantic δ13C and εNd Figure records (Sites U1403, 1051, 401, and 549). In the upper panel, there is a compilation of published δ13C for the sites. The lower panel contains the new record of U1403 εNd derived from ichthyoliths, compared to other ichthyolith records.

To better understand the evolution of Atlantic deep water movement throughout the PETM, we utilized the 4 defined time bins (Paleocene, CIE Body, CIE Recovery, and Eocene; bins defined by Penman 2016) to look at the evolution of the water masses throughout the period, without all the fluctuations, which has been determined as not impactful on paleoceanographic processes that have to do with the onset of the PETM (Figure 3.4). In the interoperation of the Atlantic neodymium isotopes, there are currently two theories explain the similarities in ε_{Nd} values between the Southern, North, and South Atlantic basins. One suggests distinct water masses with similar Nd isotopic compositions bathed the sites, suggesting that continental sources with similar isotopic compositions and basins restricted from exchanging deep water (Abbott 2016). The other theory suggests a common water mass source from the Southern Ocean bathing all sites (Thomas 2003, Thomas 2008, Batenburg 2018, Barnet, 2019).

Slight increase in ε_{Nd} between site 690 and the rest of sites in the Paleocene, CIE recovery, and Eocene, could achieved by very small amounts of radiogenic Nd, either from Caribbean sources or weathering of North Atlantic Igneous Providence basalts. During the PETM body, site 690 is slightly less radiogenic than the surrounding North and South Atlantic sites, which could possibly be due to reduced deep water formation following the initial onset of warming (Barnet et al, 2018).

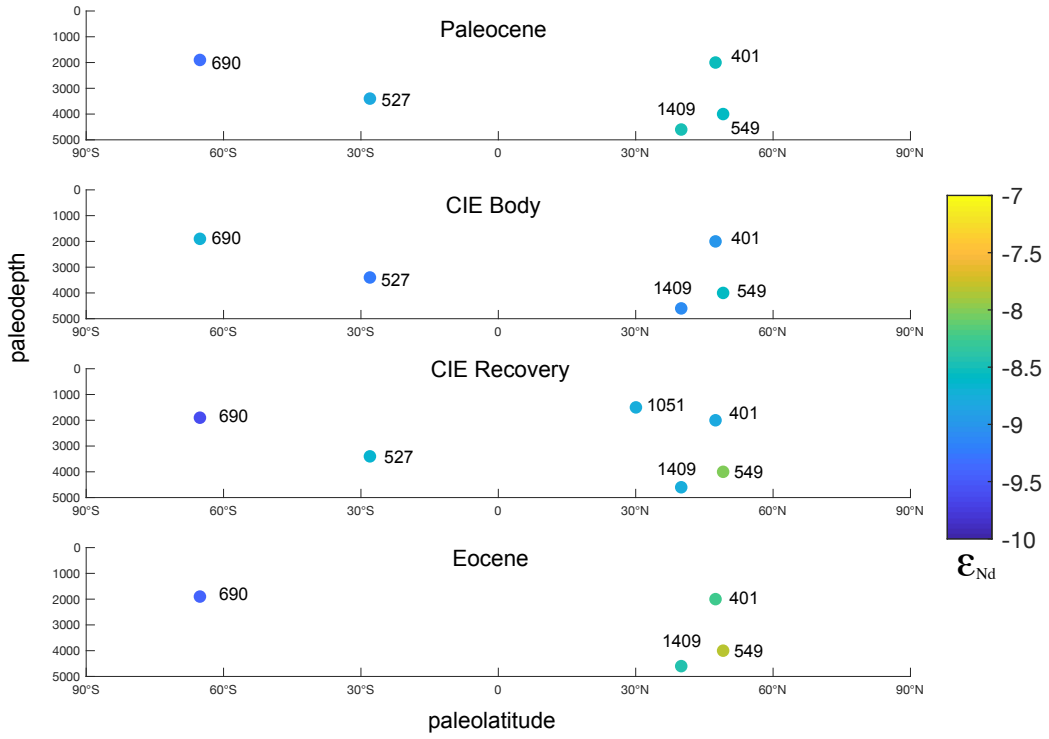

Figure 3.4 A compilation of North Atlantic, South Atlantic, and Southern Ocean εNd records (Sites U1403, 1051, 401, 527, 549, and 690; this study and Thomas 2003). All sites are plotted by paleolatitude and paleodepth. The color of the Site indicates the average εNd derived from icthyliths. The top panel contains values from 57.20 - 55.96 Ma, defined as the Paleocene time bin. The second panel covers from 55.96 - 55.89, and consists of the PETM body. The third panel covers from 55.89 -55.76, and includes the CIE recovery. The fourth bin contains values from the Eocene 55.76-55.5 (all bins defined by Penman 2016).

Conclusions

The addition of Site U1403 supports current evidence of a southern hemisphere origin of deep water formation that persisted throughout the Late Paleocene and into the Early Eocene. Though there is no evidence for temporary formation of North Atlantic deep water throughout the PETM, the ε_{Nd} records show variations among the different sites, perhaps pointing to local mixing factors or age gradients in the water. U1403

shows that even with high resolution sampling, a stable record can be obtained, leading to believe that the records with large changes are experience real local changes in bottom water composition.

References

Abbott, A. N., Haley, B. A., Tripati, A. K., & Frank, M. (2016). Constraints on ocean circulation at the Paleocene–Eocene Thermal Maximum from neodymium isotopes. *Climate of the Past*, *12*(4), 837-847.

Alegret, L., Arreguín-Rodríguez, G. J., Trasvina-Moreno, C. A., & Thomas, E. (2021). Turnover and stability in the deep sea: Benthic foraminifera as tracers of Paleogene global change. *Global and Planetary Change*, *196*, 103372.

Alexander, K., J Meissner, K., & J Bralower, T. (2015). Sudden spreading of corrosive bottom water during the Palaeocene–Eocene Thermal Maximum. *Nature Geoscience*, *8*(6), 458-461.

Barker, P. F., & Burrell, J. (1977). The opening of Drake passage. *Marine geology*, *25*(1-3), 15-34.

Batenburg, S. J., Voigt, S., Friedrich, O., Osborne, A. H., Bornemann, A., Klein, T., ... & Frank, M. (2018). Major intensification of Atlantic overturning circulation at the onset of Paleogene greenhouse warmth. *Nature communications*, *9*(1), 1-8.

Bice, K. L., & Marotzke, J. (2002). Could changing ocean circulation have destabilized methane hydrate at the Paleocene/Eocene boundary?. *Paleoceanography*, *17*(2), 8-1.

Dickens, G. R., Castillo, M. M., & Walker, J. C. (1997). A blast of gas in the latest Paleocene: Simulating first-order effects of massive dissociation of oceanic methane hydrate. *Geology*, *25*(3), 259-262.

Dickens, Gerald R. "Methane oxidation during the late Palaeocene thermal maximum." *Bulletin de la Société géologique de France* 171, no. 1 (2000): 37-49.

Frank, M., Whiteley, N., Kasten, S., Hein, J. R., & O'Nions, K. (2002). North Atlantic Deep Water export to the Southern Ocean over the past 14 Myr: Evidence from Nd and Pb isotopes in ferromanganese crusts. *Paleoceanography*, *17*(2), 12-1.

Goldstein, S. L., & Hemming, S. R. (2003). Long-lived isotopic tracers in oceanography, paleoceanography, and ice-sheet dynamics. *Treatise on geochemistry*, *6*, 625.

Haley, Brian A., et al. "The impact of benthic processes on rare earth element and neodymium isotope distributions in the oceans." *Frontiers in Marine Science* 4 (2017): 426.

Hönisch, B., Ridgwell, A., Schmidt, D. N., Thomas, E., Gibbs, S. J., Sluijs, A., ... & Williams, B. (2012). The geological record of ocean acidification. *science*, *335*(6072), 1058-1063.

Kennett, J. P., & Stott, L. D. (1991). Abrupt deep-sea warming, palaeoceanographic changes and benthic extinctions at the end of the Palaeocene. *Nature*, *353*(6341), 225-229.

Kump, L. R., Bralower, T. J., & Ridgwell, A. (2009). Ocean acidification in deep time. *Oceanography*, *22*(4), 94-107.

Kurtz, A. C., Kump, L. R., Arthur, M. A., Zachos, J. C., & Paytan, A. (2003). Early Cenozoic decoupling of the global carbon and sulfur cycles. *Paleoceanography*, *18*(4).

Lawver, L. A., & Gahagan, L. M. (2003). Evolution of Cenozoic seaways in the circum-Antarctic region. *Palaeogeography, Palaeoclimatology, Palaeoecology*, *198*(1-2), 11-37.

Lawver, L. A., Gahagan, L. M., Crowley, T. J., & Burke, K. C. (1998). Opening of Drake Passage and its impact on Cenozoic ocean. *Tectonic boundary conditions for climate reconstructions*, (39), 212.

Lunt, D. J., Dunkley Jones, T., Heinemann, M., Huber, M., LeGrande, A., Winguth, A., ... & Winguth, C. (2012). A model–data comparison for a multi-model ensemble of early Eocene atmosphere–ocean simulations: EoMIP. *Climate of the Past*, *8*(5), 1717-1736.

Martin, E. E., & Haley, B. A. (2000). Fossil fish teeth as proxies for seawater Sr and Nd isotopes. *Geochimica et Cosmochimica Acta*, *64*(5), 835-847.

Martin, E. E., & Scher, H. D. (2004). Preservation of seawater Sr and Nd isotopes in fossil fish teeth: bad news and good news. *Earth and Planetary Science Letters*, *220*(1-2), 25-39.

Martin, E. E., Blair, S. W., Kamenov, G. D., Scher, H. D., Bourbon, E., Basak, C., & Newkirk, D. N. (2010). Extraction of Nd isotopes from bulk deep sea sediments for paleoceanographic studies on Cenozoic time scales. *Chemical Geology*, *269*(3-4), 414-431.

McCarren, H., Thomas, E., Hasegawa, T., Röhl, U., & Zachos, J. C. (2008). Depth dependency of the Paleocene-Eocene carbon isotope excursion: Paired benthic and terrestrial biomarker records (Ocean Drilling Program Leg 208, Walvis Ridge). *Geochemistry, Geophysics, Geosystems*, *9*(10).

McInerney, F. A., & Wing, S. L. (2011). The Paleocene-Eocene Thermal Maximum: A perturbation of carbon cycle, climate, and biosphere with implications for the future. *Annual Review of Earth and Planetary Sciences*, *39*, 489-516.

Mountain, G. S., & Miller, K. G. (1992). Seismic and geologic evidence for early Paleogene deepwater circulation in the western North Atlantic. *Paleoceanography*, *7*(4), 423-439.

Norris, R. D., Wilson, P. A., Blum, P., Fehr, A., Agnini, C., Bornemann, A., ... & Yamamoto, Y. (2014). Site U1403. In *Proc. IODP Volume* (Vol. 342, p. 2).

Nunes, F., & Norris, R. D. (2006). Abrupt reversal in ocean overturning during the Palaeocene/Eocene warm period. *Nature*, *439*(7072), 60-63.

Pagani, M., Pedentchouk, N., Huber, M., Sluijs, A., Schouten, S., Brinkhuis, H., ... & Dickens, G. R. (2006). Arctic hydrology during global warming at the Palaeocene/Eocene thermal maximum. *Nature*, *442*(7103), 671-675.

Paytan, A., Averyt, K., Faul, K., Gray, E., & Thomas, E. (2007). Barite accumulation, ocean productivity, and Sr/Ba in barite across the Paleocene–Eocene Thermal Maximum. *Geology*, *35*(12), 1139-1142.

Penman, D. E., Hönisch, B., Zeebe, R. E., Thomas, E., & Zachos, J. C. (2014). Rapid and sustained surface ocean acidification during the Paleocene-Eocene Thermal Maximum. *Paleoceanography*, *29*(5), 357-369.

Penman, D. E., Turner, S. K., Sexton, P. F., Norris, R. D., Dickson, A. J., Boulila, S., ... & Röhl, U. (2016). An abyssal carbonate compensation depth overshoot in the aftermath of the Palaeocene–Eocene Thermal Maximum. *Nature Geoscience*, *9*(8), 575-580.

Petrizzo, M. R. (2007). The onset of the Paleocene–Eocene Thermal Maximum (PETM) at Sites 1209 and 1210 (Shatsky Rise, Pacific Ocean) as recorded by planktonic foraminifera. *Marine Micropaleontology*, *63*(3-4), 187-200.

Ridgwell, A., & Schmidt, D. N. (2010). Past constraints on the vulnerability of marine calcifiers to massive carbon dioxide release. *Nature Geoscience*, *3*(3), 196-200.

Saunders, A. D. (2016). Two LIPs and two Earth-system crises: the impact of the North Atlantic Igneous Province and the Siberian Traps on the Earth-surface carbon cycle. *Geological Magazine*, *153*(2), 201-222.

Tachikawa, K., Athias, V., & Jeandel, C. (2003). Neodymium budget in the modern ocean and paleo-oceanographic implications. *Journal of Geophysical Research: Oceans*, *108*(C8).

Talwani, M., & Eldholm, O. (1977). Evolution of the Norwegian-Greenland sea. *Geological Society of America Bulletin*, *88*(7), 969-999.

Thomas, D. J., & Via, R. K. (2007). Neogene evolution of Atlantic thermohaline circulation: perspective from Walvis Ridge, southeastern Atlantic Ocean. *Paleoceanography*, *22*(2).

Thomas, D. J., Bralower, T. J., & Jones, C. E. (2003). Neodymium isotopic reconstruction of late Paleocene–early Eocene thermohaline circulation. *Earth and Planetary Science Letters*, *209*(3-4), 309-322.

Thomas, E., & Shackleton, N. J. (1996). The Paleocene-Eocene benthic foraminiferal extinction and stable isotope anomalies. *Geological Society, London, Special Publications*, *101*(1), 401-441.

Tian, Skye Yunshu, et al. "Shallow marine ecosystem collapse and recovery during the Paleocene-Eocene Thermal Maximum." *Global and Planetary Change* 207 (2021): 103649.

Tierney, J. E., Poulsen, C. J., Montañez, I. P., Bhattacharya, T., Feng, R., Ford, H. L., ... & Zhang, Y. G. (2020). Past climates inform our future. *Science*, *370*(6517), eaay3701.

Tripati, A., & Elderfield, H. (2005). Deep-sea temperature and circulation changes at the Paleocene-Eocene thermal maximum. *Science*, *308*(5730), 1894-1898.

Tucholke, B. E., & Miller, K. G. (1983). Late Paleogene Abyssal Circulation in North Atlantic. *AAPG Bulletin*, *67*(3), 559-559.

van de Flierdt, T., Griffiths, A. M., Lambelet, M., Little, S. H., Stichel, T., & Wilson, D. J. (2016). Neodymium in the oceans: a global database, a regional comparison and implications for palaeoceanographic research. *Philosophical Transactions of the Royal Society A: Mathematical, Physical and Engineering Sciences*, *374*(2081), 20150293.

Wade, B. S., O'Neill, J. F., Phujareanchaiwon, C., Ali, I., Lyle, M., & Witkowski, J. (2020). Evolution of deep-sea sediments across the Paleocene-Eocene and Eocene-Oligocene boundaries. *Earth-Science Reviews*, *211*, 103403.

Zachos, J. C., Breza, J. R., & Wise, S. W. (1992). Early Oligocene ice-sheet expansion on Antarctica: Stable isotope and sedimentological evidence from Kerguelen Plateau, southern Indian Ocean. *Geology*, *20*(6), 569-573.

Zachos, J. C., Dickens, G. R., & Zeebe, R. E. (2008). An early Cenozoic perspective on greenhouse warming and carbon-cycle dynamics. *nature*, *451*(7176), 279-283.

Zeebe, R. E., & Zachos, J. C. (2007). Reversed deep-sea carbonate ion basin gradient during Paleocene-Eocene thermal maximum. *Paleoceanography*, *22*(3).

Zeebe, R. E., & Zachos, J. C. (2013). Long-term legacy of massive carbon input to the Earth system: Anthropocene versus Eocene. *Philosophical Transactions of the Royal Society A: Mathematical, Physical and Engineering Sciences*, *371*(2001), 20120006.